



Investigation of Performance Requirements of Full-Depth Reclamation Stabilization

Minnesota
Department of
Transportation

**RESEARCH
SERVICES
&
LIBRARY**

**Office of
Transportation
System
Management**

Jia-Liang Le, Principal Investigator
Department of Civil, Environmental and Geo- Engineering
University of Minnesota

March 2016

Research Project
Final Report 2016-09



To request this document in an alternative format call [651-366-4718](tel:651-366-4718) or [1-800-657-3774](tel:1-800-657-3774) (Greater Minnesota) or email your request to ADArequest.dot@state.mn.us. Please request at least one week in advance.

Technical Report Documentation Page

1. Report No. MN/RC 2016-09	2.	3. Recipients Accession No.	
4. Title and Subtitle Investigation of Performance Requirements of Full-Depth Reclamation Stabilization		5. Report Date March 2016	
		6.	
7. Author(s) Jia-Liang Le, Mihai Marasteanu and Rose Milavitz		8. Performing Organization Report No.	
9. Performing Organization Name and Address Department of Civil, Environmental and Geo- Engineering University of Minnesota 500 Pillsbury Dr. S.E. Minneapolis, Minnesota, 55455		10. Project/Task/Work Unit No. CTS# 2014003	
		11. Contract (C) or Grant (G) No. (c) 99008 (wo) 101	
12. Sponsoring Organization Name and Address Minnesota Department of Transportation Research Services & Library 395 John Ireland Boulevard, MS 330 St. Paul, Minnesota 55155-1899		13. Type of Report and Period Covered Final Report	
		14. Sponsoring Agency Code	
15. Supplementary Notes http://www.lrrb.org/pdf/201609.pdf			
16. Abstract (Limit: 250 words) <p>This research investigates the relationship between the mechanical properties of SFDR and the final performance of the rehabilitated pavements. The study involves two computational tools (MEPDG and MnPAVE) for the simulation of the long-term rutting behavior of pavements containing SFDR layers. Based on the simulations of three existing MnROAD cells, it is shown that for MEPDG the SFDR layer is best modeled as a bounded asphalt layer. To further investigate the applicability of MEPDG, a series of laboratory experiments are performed on cores taken from several sites constructed with different stabilizers including engineered emulsion, foamed asphalt with cement and CSS-1 with cement. The experiments include IDT creep and tension, semi-circular bending, dynamic modulus and disc compact tension tests. The measured mechanical properties are inputted into MEPDG to predict the rutting performance of these sites and it is shown that the simulated rut depth agrees well with the site measurement. However, it is found that MEPDG may suffer a convergence issue for some ranges of the values of the mechanical properties of SFDR. Due to this limitation, MnPAVE was used as an alternative. It was shown that the results simulated by MnPAVE are consistent with those obtained by MEDPG. A parametric study was performed on the three sites constructed with SFDR to determine the relationship between the long-term reliability of the rut performance and the mechanical properties of the SFDR.</p>			
17. Document Analysis/Descriptors Full depth reclamation, simulation, rutting, mechanical tests		18. Availability Statement No restrictions. Document available from: National Technical Information Services, Alexandria, Virginia 22312	
19. Security Class (this report) Unclassified	20. Security Class (this page) Unclassified	21. No. of Pages 80	22. Price

Investigation of Performance Requirements of Full-Depth Reclamation Stabilization

Final Report

Prepared by:

Jia-Liang Le

Mihai Marasteanu

Rose Milavitz

Department of Civil, Environmental and Geo- Engineering
University of Minnesota

March 2016

Published by

Minnesota Department of Transportation

Research Services & Library

395 John Ireland Boulevard, MS 330

St. Paul, Minnesota 55155-1899

This report represents the results of research conducted by the authors and does not necessarily represent the views or policies of the Minnesota Department of Transportation or the University of Minnesota. This report does not contain a standard or specified technique.

The authors, the Minnesota Department of Transportation, and the University of Minnesota do not endorse products or manufacturers. Any trade or manufacturers' names that may appear herein do so solely because they are considered essential to this report.

TABLE OF CONTENTS

CHAPTER 1: INTRODUCTION.....	1
CHAPTER 2: LITERATURE REVIEW.....	2
2.1 SFDR Purpose.....	2
2.2 SFDR Process.....	2
2.3 Stabilization Materials.....	3
2.4 Advantages of SFDR.....	4
2.5 SFDR Practicing Regions.....	5
2.5.1 Georgia – Cement Stabilizer.....	5
2.5.2 Georgia – Lime Stabilizer.....	6
2.5.3 Nevada.....	7
2.5.4 Virginia.....	7
2.5.5 Minnesota.....	8
2.6 Issues of SFDR.....	9
2.7 Laboratory Testing.....	10
2.7.1 Gyrotory Compaction.....	10
2.7.2 Resilient Modulus Testing.....	10
2.7.3 Shear Strength Testing.....	11
2.7.4 Other Tests.....	11
2.8 Summary.....	12
CHAPTER 3: INVESTIGATION OF MEPDG MODELING OF SFDR.....	13
3.1 Modeling Methodology.....	13
3.2 Input Parameters.....	13
3.2.1 Traffic Information.....	13
3.2.2 Climate Data.....	15
3.2.3 Pavement Structural Layers.....	15
3.2.4 Parameters for Thermal Cracking Analysis.....	17
3.3 Simulation of MnROAD Cells 2, 3, and 4.....	17
3.4 Summary.....	20
CHAPTER 4: MATERIAL TESTING.....	21
4.1 Specimen Preparation.....	21
4.2 IDT Test – Creep Compliance.....	22
4.3 IDT Strength Test.....	23
4.4 Dynamic Modulus.....	23
4.5 Semi-Circular Bending Test.....	27
4.6 Disc-Shaped Compact Tension Tests.....	32
4.7 Summary.....	33
CHAPTER 5: NUMERICAL MODELING OF SFDR BY MEDPG.....	35
5.1 Modeling Methodology.....	35
5.2 Pavement Structure.....	35
5.3 Dynamic Modulus Data Temperature Shifting.....	37
5.4 MEPDG Results and Comparison to Measured Rutting.....	38
5.5 Sensitivity Analysis.....	38
5.6 Limitations of MEPDG.....	39
5.7 Summary.....	40
CHAPTER 6: NUMERICAL MODELING OF SFDR BY MNPAVE.....	41
6.1 Design Inputs.....	41
6.1.1 Project.....	41

6.1.1	<i>Climate</i>	41
6.1.2	<i>Traffic</i>	41
6.1.3	<i>Structure</i>	42
6.2	MnPAVE Outputs.....	42
6.3	Modeling of 55C in MnPAVE.....	42
6.3.1	<i>Project, Climate and Traffic Inputs</i>	42
6.3.2	<i>Structure Inputs</i>	43
6.3.3	<i>Results and Comparison to MEPDG</i>	44
6.4	Modeling of TH65-C and TH65-E in MnPAVE.....	45
6.4.1	<i>Project, Climate and Traffic Inputs</i>	45
6.4.2	<i>Structure Inputs</i>	46
6.4.3	<i>Results</i>	46
6.5	Comparison.....	47
6.6	Summary.....	47
CHAPTER 7: PARAMETRIC ANALYSIS.....		49
7.1	Parametric analysis of TH55-C, TH65-C and TH65-E.....	49
7.2	Comparison.....	53
7.3	Summary.....	54
CHAPTER 8: CONCLUSIONS.....		55
REFERENCES.....		57
APPENDIX A:.....		A-1
APPENDIX B:.....		B-1
APPENDIX C:.....		C-1

LIST OF FIGURES

Figure 2.1 Inner chamber of a pavement reclaimer machine [11]	3
Figure 3.1: MnROAD pavement cross sections of cells 2, 3, and 4	16
Figure 3.2: Comparison of total rutting for MnROAD cell 2	18
Figure 3.3: Comparison of total rutting for MnROAD cell 3	18
Figure 3.4: Comparison of total rutting for MnROAD cell 4	19
Figure 4.1: SFDR specimen in IDT creep test	22
Figure 4.2: Dynamic modulus master curve for TH55-C specimens	25
Figure 4.3: Dynamic modulus master curve for TH55-F specimens	26
Figure 4.4: Dynamic modulus master curve for TH65-C specimens	26
Figure 4.5: Dynamic modulus master curve for TH65-E specimens	27
Figure 4.6: SCB test set-up	27
Figure 4.7: SCB Load versus crack opening TH55-C	28
Figure 4.8: SCB Load versus crack opening TH55-F	29
Figure 4.9: SCB Load versus crack opening TH65-C	29
Figure 4.10: SCB Load versus crack opening TH65-E	30
Figure 4.11: Elastic analysis of SCB specimen	31
Figure 4.12: DCT Template	33
Figure 5.1: TH55-C Pavement Structure	35
Figure 5.2: Temperature shift factor $\log(a(T))$ plotted against temperature and its fit by a linear function	37
Figure 6.1: TH55-C pavement structure for MnPAVE	43
Figure 6.2: MEPDG rutting prediction for TH55-C	45
Figure 6.3: TH65-C and TH65-E pavement structure for MnPAVE	46
Figure 7.1: TH55-C Design Life	49
Figure 7.2: TH55-C Rutting Reliability	50
Figure 7.3: TH65-C Design Life	51
Figure 7.4: TH65-E Design Life	51
Figure 7.5: TH65-C Rutting Reliability	52
Figure 7.6: TH65-E Rutting Reliability	52
Figure 7.7: Rutting Design Life (original E^* values)	53
Figure 7.8: 35-Year Rutting Reliability (original E^* values)	53

LIST OF TABLES

Table 2.1 Stabilizing material selection based upon base material type [17]	4
Table 2.2: Classification Requirements for SFDR Using Cement Stabilization	6
Table 2.3: MnDOT SFDR Projects	9
Table 2.4: Compaction of Base Materials	10
Table 3.1: Input traffic volume for MEPDG determined by using one-way HCA DT	13
Table 3.2: Other traffic input data	14
Table 3.3: Monthly adjustment factors	14
Table 3.4: Vehicle class distribution	14
Table 3.5: Input resilient modulus values used to model MnROAD cells 2, 3, and 4	17
Table 3.6: Comparison of MEPDG models with measured total rutting values for 05/07/2013	19
Table 4.1: Specimens used for testing	21
Table 4.2: Creep compliance (GPa^{-1})	22
Table 4.3: Poisson's ratio calculated from IDT creep test	23
Table 4.4: Tensile strength	23
Table 4.5: SCB Fracture Energy Values	32
Table 4.6: DCT Fracture Energy Values	33

Table 4.7: Fracture Energy Comparison.....	33
Table 5.1: G^* Binder Test Data Inputs	36
Table 5.2: Creep Compliance Data Inputs.....	36
Table 5.3: TH55-C Dynamic Modulus Inputs (psi).....	38
Table 5.4: Total Rutting (inches).....	39
Table 6.1: MnPAVE climate data for TH55-C.....	43
Table 6.2: 55C Dynamic Modulus Values for MnPAVE	44
Table 6.3: MnPAVE climate data for TH65-C and TH65-E	45
Table 6.4: TH65-C and TH65-E Dynamic Modulus Values for MnPAVE.....	46
Table 6.5: MnPAVE Results	47

Executive Summary

Stabilized full-depth reclamation (SFDR) is a pavement rehabilitation technique currently in practice in many states, including Minnesota. When an asphalt road is replaced, the old asphalt is ground up and mixed with water and a stabilizing agent to form a base layer for the new asphalt. The use of SFDR has environmental and economic advantages due to the elimination of the need to remove and dispose of the old asphalt. However, there is a lack of understanding on the relationship between the mechanical properties of SFDR and the final performance of the rehabilitated pavements. This research aims to develop this knowledge by investigating different experimental procedures for SFDR and numerical modeling of SFDR pavement structures.

A literature review was first conducted to review the current practice of SFDR. Next, three MnROAD cells containing a SFDR layer were modeled in the Mechanistic-Empirical Design Guide (MEPDG) to determine the best approach to numerically model a SFDR layer. It was determined that in MEPDG the SFDR should be modeled as a bound asphalt layer rather than an unbound layer.

A series of mechanical testing was performed by the University of Minnesota and by MnDOT on cores taken from several sites constructed with different stabilizers including engineered emulsion, foamed asphalt with cement and CSS-1 with cement. IDT creep and tension, semi-circular bending, dynamic modulus and disc compact tension tests were performed. The engineered emulsion specimens generally performed best in all tests.

The data from the mechanical testing was used to model the pavement sections in MEPDG. The simulation indicated that the rutting predicted by MEDPG matched closely with the rutting measured in the field. However, it was found that, for some range of the values of mechanical properties of SFDR, MEPDG could not yield a converged solution.

Due to this limitation of MEPDG, MnPAVE was used as an alternative. It was shown that the results simulated by MnPAVE are consistent with those obtained by MEDPG. A parametric study was performed on the two CSS-1 with cement specimens and the engineered emulsion specimen to determine the relationship between the long-term reliability of the rut performance and the mechanical properties of the SFDR. The simulation results showed that the engineering emulsion SFDR performed best, which is consistent with the laboratory test results.

CHAPTER 1: INTRODUCTION

Stabilized full-depth reclamation (SFDR) is a pavement rehabilitation process in which old asphalt is used to form the base for new hot mix asphalt (HMA) roads. The old asphalt is ground up and mixed with water and a stabilizing agent to form the base material. The Minnesota Department of Transportation (MnDOT) has constructed several roads using SFDR and is interested in increasing its usage. However, before MnDOT can begin widespread usage of SFDR, performance requirements specific to Minnesota for SFDR must be determined so that the structural capacity can be fully attained. The objective of the project is to determine the desired material properties for SFDR to be used as a base layer for HMA roadways in order to achieve the required overall performance, such as minimal rutting and low-temperature cracking.

The investigation consisted of several parts. First, a literature review was conducted to examine previous research on SFDR. Second, different techniques for modeling SFDR using the Mechanistic-Empirical Design Guide (MEPDG) software were explored. Third, material testing was conducted on cores taken from in-service MnDOT highways constructed with SFDR. Pavement structures were modeled in MEPDG using the properties determined from material testing and behavior was compared to MnDOT field observations for the locations the samples were taken from. The pavement structures were also modeled using MnPAVE and results were compared to those obtained from MEPDG. Finally, parametric analysis was conducted using MnPAVE to determine how MnDOT could improve its SFDR formulations.

CHAPTER 2: LITERATURE REVIEW

A literature review was conducted to provide background information and to investigate previous SFDR research. This section describes the findings, including the usage of SFDR in several states (including Minnesota) and testing that has been performed on SFDR.

2.1 SFDR Purpose

SFDR is a pavement rehabilitation method. It serves two main purposes: 1) to reuse asphalt on a road that needs to be rehabilitated and 2) to provide a base for new asphalt.

SFDR is used to correct structural deficiencies in pavement [1]; these deficiencies include deep rutting, load-associated cracks, thermal cracks, reflection cracks, and maintenance patches such as spray, skin, potholes, and deep hot mix [2]. SFDR can correct inconsistencies in the aggregate base as well as in the asphalt layers [3]. In contrast to structural deficiencies are functional deficiencies, such as pavement surface texture. Since cold recycling methods are used to correct for most functional deficiencies, SFDR would be a poor choice as a type of pavement recycling process for this type of deficiency [1]. To determine if a pavement is failing due to structural deficiencies, it is suggested to use the following types of pavement field testing before proceeding with SFDR processes: cores, depth checks and falling weight deflectometer tests [1]. It should be emphasized that not all road failure cases may be resolved with SFDR.

Public roadways are the most common places where SFDR is performed. Since total rehabilitation of a roadway cannot be done without some form of traffic control, SFDR is more often used for long stretches of rural roads [4, 5]. The SFDR process is moving towards other fields of application however; private and regional airports as well as parking lots are being rehabilitated through the use of SFDR [6]. Since SFDR is simultaneously being developed as a technology and applied to roadway systems, there is much potential for future success of SFDR in pavement rehabilitation applications.

2.2 SFDR Process

When a Department of Transportation and contractor have agreed that SFDR is the best option for road rehabilitation, there is a general process that is followed to complete the SFDR process. This process may be described in six steps [7]:

1. Mix design selection
2. Pulverization
3. Introduction and blending of additives
4. Shaping of the mixed material
5. Compaction
6. Application of a surface or a wearing course

A more detailed example of an SFDR road rehabilitation process may be similar to the following example taken from a report by the Georgia Department of Transportation (GDOT) on a SFDR project in its state [8]:

1. On the first pass of the reclaimer, the pavement structure was pulverized to begin the SFDR process.

2. On the second pass, water was added to the SFDR and blended well.
3. On the third pass, Portland cement was added at a ratio of 6% by weight to the pulverized dry material.
4. The reclaimer made two more passes to blend the SFDR with the cement. The final blend was a homogeneous stabilized SFDR base.
5. Compaction of the SFDR base was achieved by passing a vibratory smooth drum roller over the stabilized base. Two passes were made initially.
6. Additional water was added to the stabilized base as necessary.
7. Further compaction was achieved with four passes of a pneumatic roller.
8. A minimum compaction of 98% of the maximum dry density was achieved.
9. A motor grader then passed over the SFDR base to grade the SFDR and achieve the proper slope of the road.
10. The stabilized and compacted base was then sealed with a bituminous prime coat of 0.7 L/m². The coat was allowed to seal for seven days.
11. Paving operations followed the completion of the stabilized base.

Although the reclamation depth was not specified in the GDOT example, typical depths may be anywhere from 50 - 300 mm (2 - 12 in) [9]. The reclamation depth used is based upon the proportion of pavement to subgrade material. This proportion may change based on the specification of the state in which SFDR is performed, but typical ratios include 50% Recycled Asphalt Pavement (RAP) to 50% base material by weight and 75% RAP to 25% base material by weight [10]. The inner chamber of a pavement reclaimer machine is shown in Fig. 2.1.

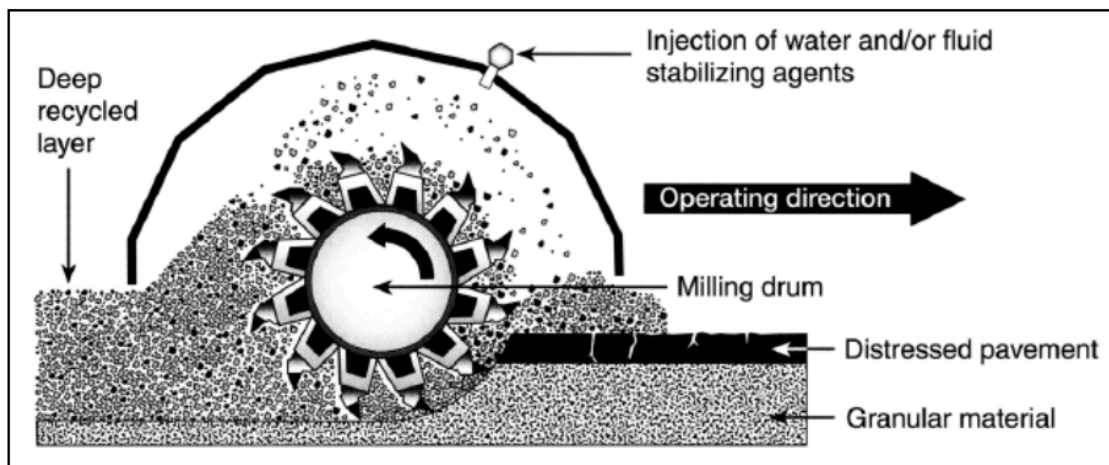


Figure 2.1 Inner chamber of a pavement reclaimer machine [11]

2.3 Stabilization Materials

MnDOT initially suggested the use of cement and emulsion as stabilizing additives for SFDR base used for Minnesota roadways [12]. Although cement and emulsion had been suggested as the two additives to be used for this research project, it was later determined that the stabilization materials should be determined by the agency conducting the SFDR project. The choice of a specific additive is based upon the type of existing pavement as well as the type of existing

aggregate base of a roadway, and is not restricted solely to cement and emulsion. Common stabilizing additives include [13, 14 & 15]:

- Asphalt emulsion
- Expanded/foamed asphalt
- Calcium chloride
- Portland cement
- Fly ash
- Lime

Both dry cement and cement slurry have been used to stabilize SFDR [16]. Dry cement is more conventional, but could lead to fugitive cement dust when spreading. Cement slurry has recently been used to solve the problem of fugitive cement dust. Although the slurry did prevent dust issues, SFDR stabilized with cement slurry has slightly lower strength values than SFDR stabilized using dry cement [16].

A study conducted by the Virginia Department of Transportation (VDOT) compiled a chart, shown in Table 2.1, of different types of stabilizing and base materials. This table could be used in the selection of a stabilizing material when the base material type is known.

Table 2.1 Stabilizing material selection based upon base material type [17]

Material Type	Well-graded Gravel	Poorly graded Gravel	Silty Gravel	Clayey Gravel	Well-graded Sand	Poorly graded Sand	Silty Sand	Clayey Sand	Silt, Silt with Sand	Lean Clay	Organic Silt/Organic Lean Clay	Elastic Silt	Fat Clay, Fat Clay with Sand
USCS	GW	GP	GM	GC	SW	SP	SM	SC	ML	CL	OL	MH	CH
AASHTO	A-1-a	A-1-a	A-1-b	A-1-b or A-2-6	A-1-b	A-3 or A-1-b	A-2-4 or A-2-5	A-2-6 or A-2-7	A-4 or A-5	A-6	A-4	A-5 or A-7-5	A-7-6
Emulsion FDR, Best if SE > 30 and P ₂₀₀ < 20													
Foamed asphalt, P ₂₀₀ 5% to 20% and follow maximum density gradation													
Portland cement, PI < 10													
Lime, PI > 10 and P ₂₀₀ < 25 or PI 10-30 and P ₂₀₀ > 25, SO ₄ in clay < 3,000 ppm													

Shaded cells indicate recommended conditions.
 USCS = unified soil classification system; AASHTO = American Association of State and Highway Transportation Officials; FDR = full-depth reclamation; SE = sand equivalent; P₂₀₀ = percent passing No. 200 sieve; PI = plasticity index; ppm = parts per million.
 Source: The recommendations in this table are from Thomas, T. (2010). Mix Designs for FDR, CIR, and HIR. Paper presented at the Northeast and Mid-Atlantic States In-Place Recycling Conference, Harrisburg, PA, August 24-26.

2.4 Advantages of SFDR

Costs of road rehabilitation materials have risen at a rate of approximately 70% over a two-year span [1]. This poses a significant challenge for departments of transportation who wish to rehabilitate roadways. This economic challenge has been overcome in the past few years by the

use of SFDR. As well as providing a cheaper alternative for rehabilitation of roadways, SFDR offers many other advantages [2, 22, 23, 24 & 25]:

- Reduction in total cost
- Reduction in frost susceptibility
- Improvement of pavement structure without changing basic roadway geometry
- Improvement of ride quality
- Restoration of old pavement to desired profile
- Restoration of crown and slope
- Elimination of existing wheel ruts
- Elimination of potholes, irregularities and rough areas
- Elimination of alligator, transverse, longitudinal and reflection cracks
- Elimination of air quality problems from dust, fumes and smoke
- Elimination of initial pavement disposal
- Reconstruction of shoulders
- Accommodation of pavement widening projects
- Conservation of materials and energy
- Minimization of traffic interruptions
- Preservation of natural resources

2.5 SFDR Practicing Regions

There are multiple states and countries that practice SFDR. Several of the most prominent SFDR practicing states will be reviewed in this report including Georgia, Nevada, and Virginia as well as Minnesota. The following list should by no means be considered a comprehensive list of all regions practicing SFDR.

A discussion of each region's SFDR practices will be provided in the following sections. Parameters of the region that are similar to Minnesota parameters will be highlighted. The discussions will include reasons why SFDR was chosen as a rehabilitation process, the different stabilizing materials used, any construction highlights that may aide in understanding the SFDR process, and any problems detected by the use of SFDR.

2.5.1 Georgia – Cement Stabilizer

The Georgia Department of Transportation (GDOT) is in the process of developing cement-stabilized reclaimed base (CSRB). CSRB is an SFDR base that is produced by using Portland cement as a stabilizer for a sand-clay existing base. Once the base has been stabilized, hot-mix asphalt is laid on top of the base to complete the roadway [3]. GDOT is the first transportation agency to develop a specification for the use of CSRB. This specification is summarized in Table 2.2. Since CSRB uses cement as a stabilizer, the final base course has reduced permeability and is able to keep moisture out. This reduction in permeability means that the base maintains a high level of strength and stiffness even when it has become saturated [3]. CSRB also allows for thinner pavement sections because of its high strength as a base.

Table 2.2: Georgia Standard Specification 814.02 – Classification Requirements for SFDR Using Cement Stabilization [22]

<u>Soil Property</u>	<u>GDOT Specification</u>
Clay Content (%)	5-25
Volume Change (% max.)	18
Liquid Limit (max.)	25
Plasticity Index (max.)	10
% Passing #200 Sieve	0-30

GDOT has rehabilitated many roadways by the use of SFDR for the following reasons: normal vehicular traffic causing load-fatigue cracking of the pavement surface, water penetrating the granular base, underlying clay retaining water and deforming the base, and heavy timber trucking and overweight farm equipment causing deterioration [3]. GDOT would have conventionally recommended a complete removal of the existing asphalt pavement for the roadways with the aforementioned issues. However, SFDR offered a less expensive alternative; therefore GDOT pursued SFDR as a pavement rehabilitation process [3].

The use of SFDR by GDOT allowed for a total cost reduction of 42% in comparison to complete reconstruction of pavement structures using conventional rehabilitation methods [3]. GDOT determined that the optimal mixing ratio needed for stabilization was 6% cement by weight of the dry existing base course [3]. This addition of cement achieved the desired level of unconfined compressive strength of 3,100 kPa [3]. GDOT also determined that the optimal moisture content of the SFDR was 11.6% [3]. Review of the pavement structures after one year of project completion revealed that a few problems were caused by the use of SFDR. Minimal cracking occurred due to excessive amounts of cement being used to stabilize the base. Also, minimal rutting had occurred from the base not being fully stabilized [3].

2.5.2 Georgia – Lime Stabilizer

Reconstruction of a Georgia roadway occurred in April of 2006 [22]. It was determined that the roadway was to be repaired by the use of SFDR. Base and pavement cracking were caused by instability in the underlying subgrade material that consisted mostly of clay-silt soils [22]. The use of lime as a soil stabilizer is a well-known construction technique and was used in this project to stabilize the underlying base course.

Soil stabilization occurs when lime is added to a reactive soil. This addition of lime generates long-term strength through a chemical reaction that produces calcium silicate hydrates and calcium aluminate hydrates. These hydrates provide strength to the pavement structure [23]. This reaction may occur for longer than a decade as long as sufficient amounts of lime are present (pH > 10) [23]. The Thompson procedure states that most fine-grained soils, such as the clay-silt in the SFDR, may be stabilized with 3-10% lime on a dry soil weight basis [24]. The optimal mixing ratio determined was 6% lime by volume [22]. GDOT also determined that the optimal moisture content for the SFDR base was 13% by weight [22].

During construction of the roadway, the lime was well mixed to achieve the benefits of the lime stabilizer. Some of these benefits included high and long lasting strength gains, increase in

resilient modulus values, improvements in shear strength, plasticity reduction, reduction in moisture-holding capacity, and improved stability [22]. Soil and falling weight deflectometer testing were performed by GDOT before and after the SFDR process and the results indicated substantial improvement in the structure of the pavement and the subgrade [22]. No problems as a result of the SFDR process were reported for Georgia's use of lime.

2.5.3 Nevada

The Nevada Department of Transportation (NDOT) uses both cold-in-place recycling (CIR) and SFDR pavement rehabilitation methods as a way to reduce the cost of roadway rehabilitation projects. The department has saved over \$600 million over the past 20 years by its use of SFDR and CIR [1]. NDOT estimates that it saves \$330,000 per centerline mile when it uses SFDR or CIR recycling techniques rather than complete pavement reconstruction [1]. 96% of all roadways in Nevada are considered to be a "good" ride quality, which is the highest percentage of "good" ride quality roads in the nation [1]. Nevada experiences reflective cracking of its pavement. NDOT has established SFDR as the conventional method to fix pavement structures with this type of cracking.

NDOT has developed some special techniques for its implementation of SFDR. After pulverization of the pavement, the material must have a 95% to 100% passing by mass rate for a 2-in. sieve [1]. NDOT uses cement as a stabilizer at a rate of 2% cement by weight of the reclaimed material. In some regions of Nevada, the climate is more severe, and so the cement content was reduced to 1.5%; this reduction in cement proportion prevented long-term transverse cracking [1]. The pulverized material is compacted to no less than 95% relative maximum density and then is coated with seal coat to allow for hydration of the cement [1]. After the base course has cured, a 3 ½ - 5 ½ inch plant-mix bituminous surface is laid over the processed base [1].

NDOT has completed almost 900 miles of SFDR since 1985 [1]. Since it has such a long history of practicing SFDR, it is able to record great data on the longevity of this process. Multiple 10-year performance reports indicate that most NDOT SFDR projects performed well. Minor cracking was encountered and failed pavements had typically occurred for reasons other than the use of SFDR [1]. 10-15 year reports begin to show the fatigue of the pavement. Most pavement structures performed well, but several projects exhibit transverse or fatigue cracking [1]. It was determined that the transverse cracking occurred because of the relative stiffness of the SFDR base [1]. Selective core tests were performed and it was shown that the cracking had been reflected through the SFDR layer. Non-wheel path longitudinal cracking was also observed to be a result of inadequate compaction of the SFDR during construction [1]. Therefore, good construction techniques are imperative to the success of an SFDR project. After 15 years of use, nearly all SFDR projects experienced reflective cracking and some have been rehabilitated again.

2.5.4 Virginia

The Virginia Department of Transportation (VDOT) constructed three trial SFDR sections in the summer of 2008 [21]. These trial sections each used a different agent to stabilize the FDR. The stabilizing agent used in the first and second sections of roadway was Portland cement, the second section used a combination of asphalt emulsion and foamed asphalt binder to stabilize the FDR.

The VDOT study concluded that SFDR should be used in the future as a roadway rehabilitation option for its cost savings potential. VDOT estimates that it could potentially save \$1.42 million per year if it used SFDR on roads that qualify for rehabilitation [21]. VDOT also concluded that the structural capacity of pavement rehabilitated by the use of SFDR is dependent on both the chosen stabilizing agent, as well as time [21]. Estimation of the structural capacity of a newly rehabilitated road structure could not be accurately completed immediately after a project is completed. VDOT noticed change in the structural capacity of the pavement for at most two years after project completion, however, core sample testing typically showed no difference in structural capacity of 5 month samples and 33 month samples [21]. Laboratory tests showed that there was no statistically significant difference between the resilient modulus values of FDR stabilized with foamed asphalt and FDR stabilized with emulsion [21].

2.5.5 *Minnesota*

Minnesota currently practices SFDR and has been for many years. Since there is history of SFDR in Minnesota, it will be explored in this section. This data will be most valuable to this research project. Different articles were reviewed and their results are shared in the following paragraphs.

MnDOT currently allows the use of RAP as Class 7 aggregate base. Attia et al. conducted research on the effect of freeze-thaw and severe moisture conditions on the structural capacity of pavement base layers [25]. They studied many different types of pavement base including: one sample of 100% RAP, one sample of virgin aggregate, and three samples of SFDR. The research team performed laboratory testing on the materials and measured properties such as the resilient modulus (MR) and shear strength after conditioning the samples. The samples were compacted using a Supervave gyratory compactor. Resistance to abrasion and degradation of the samples was tested using the Micro-Deval test. Structural capacity was determined by testing the MR of the samples following the National Cooperative Highway Research Program (NCHRP) 1-28A protocol. The triaxial shear test was used to determine shear strength of the samples.

Attia et al. concluded that the MR for all RAP material was higher than that of the virgin aggregate, specifically Class 5 [25]. The MR of the material was also found to be dependent on the confining pressure. The research team further concluded that there was no significant loss of MR due to freeze-thaw conditioning for the tested samples [25]. This effect was only significant at low confining pressures. As the pressure increased, this correlation ceased to exist. Therefore, RAP can be considered as a viable option for use as a pavement base layer.

Kim and Labuz recently published a report on the performance characteristics of base material produced from RAP and aggregate [26]. Their research aimed to determine the strength and deformation characteristics of the base material they were studying. Since the base material they were studying are similar to the base materials studied for this research project, their mechanical test methods are valuable.

Kim and Labuz concluded that at least two times greater permanent deformation occurred in specimens with RAP than the 100% aggregate material; as RAP increases, more permanent

deformation occurs [26]. They also concluded that permanent strain and energy loss reached a constant value as the number of cycles increased in a triaxial test for shear strength [26]. They reported that the order of permanent strain and energy loss for the first five cycles was the same as the order for the entire cycling. This indicates that more permanent strain and energy loss occurs when the proportion of RAP is increased [26].

Kim and Labuz also investigated Young’s modulus and found that for the first five cycles of a triaxial shear strength test, the aggregate specimen was the stiffest, but the 25% aggregate – 75% RAP specimen was the stiffest after 5000 cycles [26]. Kim and Labuz concluded that when considering stiffness and strength of the base course material, 50% aggregate and 50% RAP mixtures perform similar to 100% aggregate base that has been properly compacted [26].

MnDOT has completed many SFDR construction projects on different trunk highways (TH) and county roads (CR) throughout the state of Minnesota. These projects and their respective mix designs are displayed in Table 2.3. All of these mix designs were determined by American Engineering Testing (AET) according to the Road Science specification *Guidelines for Asphalt Emulsion Full Depth Reclamation (FDR) and Granular Base Stabilization (GBS)* [27].

Table 2.3: MnDOT SFDR Projects

Road	Mix Design
CR 30	4 to 5 % Emulsion
TH 55	4 to 5 % Emulsion
TH 65	1.5 % Cement and 3 to 3.5 % Emulsion
TH 70	1.5 % Cement and 4 to 5 % Emulsion

2.6 Issues of SFDR

It is apparent that SFDR processes have multiple advantages such as the ones listed previously in this report. The list of advantages may be extensive, but the SFDR process still has issues. Some of these issues were seen in Georgia and Nevada’s implementation of SFDR in its roadways. NDOT has found after 20 years of SFDR practice, that the greatest lifetime of a SFDR rehabilitated pavement structure is 15 years. After 15 years, or less if poor construction techniques were used, different forms of fatigue begin to appear.

Georgia did not report many problems with the performance of its lime SFDR pavement structures, but this is likely due to a shorter time of roadway observation. The use of cement as a stabilizer in Georgia did show signs of fatigue. Minimal cracking occurred due to excessive amounts of concrete being used and minimal rutting occurred due to the base not being fully stabilized.

NDOT experienced cracking of the SFDR base course, which was often reflected to the pavement surface. Transverse cracking and fatigue cracking has also been noticed in Nevada’s SFDR pavement structures. Even though NDOT has over 20 years of SFDR data, it still encounters cracking problems in its structures. Poor construction techniques may also lead to cracking and fatigue issues; therefore a well-informed contractor is imperative to successful SFDR implementation.

One of the main issues with SFDR is that it is difficult to come up with a mix design formula since the existing base materials vary from site to site. On the other hand, few studies have been performed to investigate the desirable mechanical properties of SFDR that should be achieved in order to ensure a good performance of the upper pavement layer.

2.7 Laboratory Testing

Understanding the mechanical performance of the SFDR base is critical for determining optimal design parameters. To determine the mechanical properties of the SFDR, it is necessary to test SFDR samples in a laboratory to determine specifications for pavement materials such as modulus and shear strength values. After a review of the literature, it was found that fracture energy tests of SFDR have not yet been performed by other research agencies. Fracture energy tests are very important for determining the low-temperature cracking potential of SFDR, so it is suggested that fracture energy tests be performed in the proposed research. This section describes some of the current tests performed on SFDR laboratory samples.

2.7.1 Gyratory Compaction

Research samples are typically compacted using a gyratory compactor [1, 22, 25 & 26]. Samples prepared using gyratory compaction methods more closely resemble densities of aggregates measured in the field. Table 2.4 displays how the gyratory compactor achieved higher densities in comparison to the proctor method.

Table 2.4: Compaction of Base Materials [26]

Soil Identification Letter	Description	Proctor		Gyratory	
		Maximum Dry Density (kg/m ³)	Optimum Moisture Content (%)	Maximum Dry Density (kg/m ³)	Optimum Moisture Content (%)
S	In-situ Blend, CR 3	1984	9	2032	7.8
T	100% Aggregate, CR 3	2000	10	2032	8.8
U	75% Aggregate - 25% RAP, CR 3	2000	10	2032	8.7
V	50% Aggregate - 50% RAP, CR 3	1952	9.5	2032	8.0
W	25% Aggregate - 75% RAP, CR 3	1920	8.5	2032	7.2
X	In-situ Blend, TH 23	2000	7	2080	5.4
Y	In-situ Blend, TH 200	2096	6.5	2144	5.7
Z	In-situ Blend, TH 5	1984	8.5	2112	6.6

2.7.2 Resilient Modulus Testing

Resilient modulus (MR) tests are conducted following the National Cooperative Highway Research Program 1-28A test protocol [26]. In this procedure, cycles of repeated axial stress are applied to a laboratory sample at a given confining pressure within a conventional triaxial cell. From the report of Kim and Labuz, MR was seen to increase with increase of confining pressure [26]. MR also showed little change for changes in deviator stress. Kim and Labuz reported that the MR test results showed an increase in MR with the addition of RAP [26].

Kim and Labuz have shown in their report that the MR value is dependent on the stress applied during the loading of the samples. The research team explored many different models to find one that most accurately describes their data [28-32]. The model, which most accurately matches their data, is given by Eq. 2-1 [28 & 29]:

$$M_R = k_1 \cdot \left(\frac{\sigma_3}{P_a} \right)^{k_2} \quad (2-1)$$

where k_1, k_2 = regression coefficients

P_a = atmospheric pressure (0.101 MPa)

σ_3 = confining pressure

This equation fit the data well if the regression coefficient $k_2 = 0.50$. Kim and Labuz also reported that MR increased as the confining pressure increased. They described this relationship with a square root dependence in Eq. 2-2 [26]:

$$\frac{M_R}{P_a} = k \cdot \left(\frac{\sigma_{mean}}{P_a} \right)^{0.5} \quad (2-2)$$

where $\sigma_{mean} = (\sigma_1 + \sigma_2 + \sigma_3)/3$ = confining pressure

P_a = atmospheric pressure (0.101 MPa)

k = regression coefficient

2.7.3 Shear Strength Testing

The report by Kim and Labuz also included shear strength testing of the samples. Their samples were tested at confining pressure values of 34.5 kPa and 69 kPa [30]. Determination of the friction angle (ϕ) and cohesion (c) which was used by Kim and Labuz is given in Eq. 2-3 and Eq. 2-4 [26]:

$$\sigma_{1f} = 2c\sqrt{K_p} + K_p\sigma_3 \quad (2-3)$$

$$K_p = \frac{1 + \sin \phi}{1 - \sin \phi} \quad (2-4)$$

where σ_3 = confining pressure

σ_{1f} = confining pressure + deviator stress

Cyclic triaxial testing is often conducted to evaluate samples for their shear strength. For example, Kim and Labuz used a 5000 cycle test to evaluate their samples.

2.7.4 Other Tests

Fracture energy may be determined by either the semi-circular bend (SCB) test or the disc compact tension (DCT) test. The SCB test has been shown to have higher variability in comparison to the DCT, therefore the DCT is recommended over the SCB. However, since the preparation of DCT specimen could possibly damage the SFDR material, the SCB test may serve as a substitute for determination of fracture energy. Creep compliance of tested samples may be determined by using the indirect tensile test (IDT). Stiffness of the SFDR samples may be determined by running the dynamic modulus (E^*) test.

2.8 Summary

One of the biggest challenges SFDR faces is overcoming the variability of field conditions. Since each road rehabilitation project has different conditions such as existing pavement, existing soil and environmental conditions, determining the correct mixing ratio of additives used in SFDR is often difficult. Difficulty also lies in the mechanics of testing these stabilized bases. Lab result tests may indicate that a certain mixing ratio is projected to perform best in the field. However, field-testing may show that a different mixing ratio performs better.

Methods for testing SFDR are similar to methods used to test pavement materials. Resilient modulus values indicate the stiffness of the material and therefore determination of this value is imperative to this research study. Other laboratory tests of interest include shear strength testing, fracture energy testing, and creep compliance testing. A review of the literature, however, did not find any reports on fracture energy tests performed on Minnesota SFDR. Therefore, this research project included fracture energy tests for the SFDR samples.

After a review of the literature, it was determined that the desired mechanical properties for SFDR are not well defined. Trial and error methods are typically used when designing a mix for an SFDR project, but there is no general consensus on what makes a good mix design. With an aim of developing a practical method for determining the mix design of SFDR, this research will investigate the relationship between the mechanical properties of the SFDR and its long-term performance through a series of parametric studies. The study will use well-established numerical tools, which are currently adopted by MnDOT. The numerical model will be further validated by a set of experiments on the SFDR cores extracted from several existing SFDR projects in Minnesota.

CHAPTER 3: INVESTIGATION OF MEPDG MODELING OF SFDR

Techniques for modeling pavement with an SFDR layer in the MEPDG software were explored to determine the best way to proceed with the research. MnROAD cells 2, 3 and 4 were used in the investigation because detailed design and condition data was available.

3.1 Modeling Methodology

In this study, the MEPDG software was first used to model pavement structures. MEPDG version 1.100, released on August 31, 2009, was used for the simulations. The pavement structure was modeled as a flexible pavement. There are three possible approaches to modeling SFDR pavement layers in MEPDG: as a bound asphalt layer, as a stabilized base layer, and as an unbound granular layer. Previous research by Velasquez et al. [33] showed that modeling SFDR as a stabilized base layer was not successful so this investigation proceeded with modeling SFDR only as a bound asphalt layer and an unbound granular layer.

MEPDG simulations were run for a design life of 20 years. The rutting results were compared with the available five years of field data for each cell.

3.2 Input Parameters

The following input parameters are required to model SFDR in MEPDG:

- Traffic information
- Climate data
- Pavement structural layers
 - Asphalt concrete layers
 - Granular layers
 - Subgrade layers
- Parameters for thermal cracking analysis

3.2.1 Traffic Information

Traffic data was obtained from the MnROAD database. Since all of the cells were constructed in October of 2008, and they are all adjacent to one another, the same input traffic data was used for each of the cells. The MnROAD mainline traffic calculator was used to determine the Average Annual Daily Truck Traffic (AADTT), which is a measure of the fraction of trucks that are class four or higher. The MEPDG inputs two-way AADTT traffic and the MnROAD mainline traffic calculator outputs one-way Heavy Commercial Average Daily Traffic (HCADT). Two-way AADTT is equal to two times one-way HCADT. The following time period was entered into the calculator: October 15, 2008 – May 15, 2013. The traffic volume results are reported in Table 3.1.

Table 3.1: Input traffic volume for MEPDG determined by using one-way HCADT as given by MnROAD mainline traffic calculator

HCADT	AADT
1,987	3,974

The rest of the input traffic data was obtained from MnDOT. This data is summarized in Tables 3.2, 3.3, and 3.4. Table 3.3 contains the monthly adjustment factors for truck traffic. The monthly adjustment factors account for variability in the truck traffic distribution. Additionally, the vehicle class distribution is reported in Table 3.4. The traffic growth factor was set to 3%, and the remaining traffic input data required by the MEPDG was kept as the default values.

Table 3.2: Other traffic input data

# Lanes	2
% trucks in design direction	50
% trucks in design lane	77.24
Operational Speed	60 mph

Table 3.3: Monthly adjustment factors

Month	Class 4	Class 5	Class 6	Class 7	Class 8	Class 9	Class 10	Class 11	Class 12	Class 13
January	1.6	1.02	1.24	1.24	1.25	0.93	0.93	0.95	0.95	0.95
February	1.44	0.93	1.17	1.17	1.15	0.86	0.86	0.86	0.86	0.86
March	1.31	0.96	1.12	1.12	1.11	0.87	0.87	0.92	0.92	0.92
April	0.99	0.89	0.89	0.89	0.97	0.82	0.82	0.86	0.86	0.86
May	0.81	0.85	0.76	0.76	0.84	0.79	0.79	0.86	0.86	0.86
June	0.75	0.87	0.71	0.71	0.77	0.79	0.79	0.75	0.75	0.75
July	0.67	0.83	0.7	0.7	0.72	0.82	0.82	0.8	0.8	0.8
August	0.68	0.83	0.66	0.66	0.72	0.78	0.78	0.76	0.76	0.76
September	0.71	0.76	0.65	0.65	0.72	0.8	0.8	0.75	0.75	0.75
October	0.68	0.77	0.64	0.64	0.83	0.73	0.73	0.7	0.7	0.7
November	0.96	0.88	0.86	0.86	1.07	0.87	0.87	0.82	0.82	0.82
December	1.4	1	1.09	1.09	1.25	0.9	0.9	0.76	0.76	0.76

Table 3.4: Vehicle class distribution

Vehicle Class	Distribution (%)
Class 4	3.34
Class 5	14.06
Class 6	4.10
Class 7	0.76
Class 8	4.10
Class 9	67.55
Class 10	3.19
Class 11	2.05
Class 12	0.61
Class 13	0.23
Total	100.00

3.2.2 Climate Data

The MEPDG assigns moisture and temperature profiles to the pavement structures using a model referred to as the Enhanced Integrated Climatic Model (EICM) [33]. This model creates profiles by referencing meteorological data from a selected weather station. MEPDG has approximately 800 weather stations in its database, with 15 of those being in the state of Minnesota. The MnROAD research facility is closest to the St. Cloud weather station, but lies approximately equal distance between the St. Cloud and Minneapolis-Saint Paul Airport (MSP) weather stations. Since the data of the St. Cloud weather station is missing, the MSP weather station was chosen as the input for climate data for all three cells. MEPDG also requires the input of a water table depth. A water table depth of 10 feet was used for this study as indicated by the United States Geological Survey website [34].

3.2.3 Pavement Structural Layers

MEPDG has three levels of input for pavement layers. Level three is the most basic level and uses many default parameter values. Level three output consists of basic performance indicators. Level two represents an intermediate level, while level one is the most advanced. Level one requires significantly more information about the materials used in the pavement layers and produces the most accurate performance indicators. Three types of layers were used to build the pavement structure: asphalt concrete layer, granular layer, and subgrade layer. Level one was chosen for the asphalt concrete layers. The input parameters are: asphalt mixture complex modulus $|E^*|$ and asphalt binder complex shear modulus $|G^*|$.

For the granular layers, level three was used that requires resilient modulus (MR) values. Level one was not used since MEPDG uses a two-dimensional finite element program that has not yet been calibrated for Minnesota conditions. Level two requires California Bearing Ratio (CBR), Layer Coefficient, etc. MnDOT did not collect this data. Level three was also used to model the subgrade layers for similar reasons

In summary, the following input parameters were used to model the pavement structure of cells 2, 3, and 4:

- Asphalt Concrete Layer Input Values (Level 1 Input):
 - Layer Thickness
 - Asphalt Mix Properties
 - Values of complex modulus $|E^*|$ at prescribed frequencies and test temperatures are required.
 - Asphalt Binder
 - Values of the binder complex shear modulus $|G^*|$ at prescribed temperatures and frequencies are required.
 - General Asphalt Concrete Input – Default Values Used
 - Reference temperature = 70 °F
 - Poisson's ratio: $\nu = 0.35$
 - Effective binder content = 11.6 %
 - Air voids = 7 %
 - Total unit weight = 150 lb/cubic foot

- Thermal conductivity = 0.67 BTU/hr-ft-°F
 - Heat capacity = 0.23 BTU/lb-°F
- Granular Layer Input Values (Level 3 Input):
 - Layer Thickness
 - Resilient Modulus (M_R)
 - Reported at optimum moisture content
 - Aggregate Properties
 - AASHTO soil classification used to select aggregate type
 - Default values assigned to the aggregate type selected
 - General Granular Layer Inputs – Default Values Used
 - Poisson’s ratio: $\nu = 0.35$
 - Coefficient of lateral pressure: $K_0 = 0.5$
- Subgrade Layer Input Values (Level 3 Input)
 - The subgrade layer input types are the same as the granular layer inputs.

Figure 3.1 describes the pavement structure for each of the three cells used in the analysis and the input values used to model them in the MEPDG. More specific data such as complex modulus $|E^*|$ and binder complex shear modulus $|G^*|$ values may be found in Appendix A of this report. Resilient modulus values are summarized in Table 3.5. All input values for the MnROAD cells were obtained from MnDOT laboratory tests.

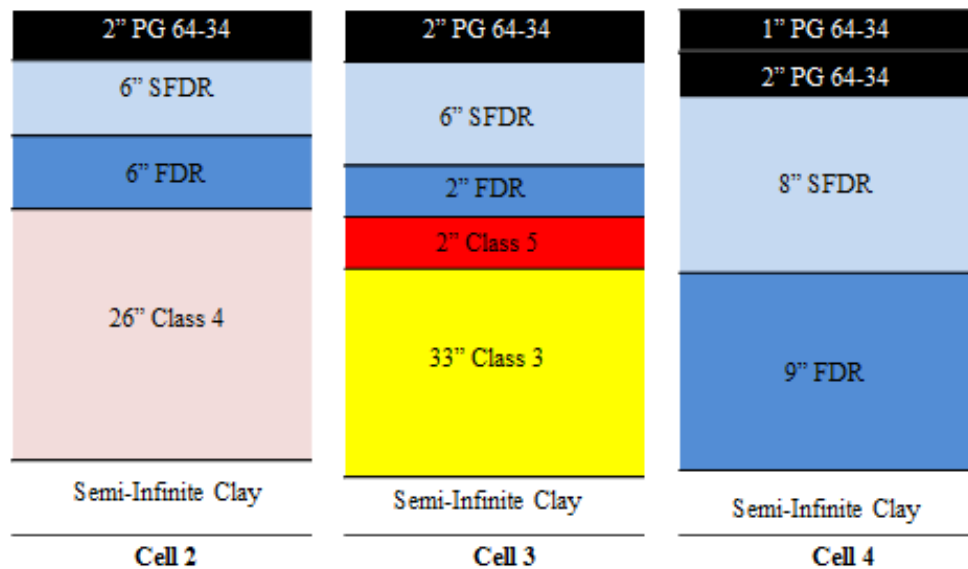


Figure 3.1: MnROAD pavement cross sections of cells 2, 3, and 4

Table 3.5: Input resilient modulus values used to model MnROAD cells 2, 3, and 4

Layer Number	Cell 2 M_R Values	Cell 3 M_R Values	Cell 4 M_R Values
1	N/A	N/A	N/A
2	87,500 psi	82,600 psi	N/A
3	37,500 psi	45,000 psi	85,500 psi
4	30,000 psi	30,000 psi	65,000 psi
5	14,000 psi	23,000 psi	14,000 psi
6		14,000 psi	

3.2.4 Parameters for Thermal Cracking Analysis

Level three was used to model thermal cracking in the surface asphalt layer. Asphalt mixture creep compliance values were determined from asphalt binder test data used to obtain the performance grade (PG) of the binder. MnDOT did not perform asphalt mixture IDT creep and strength tests that are required for level one input.

3.3 Simulation of MnROAD Cells 2, 3, and 4

Each of the three MnROAD cells was modeled twice in MEPDG – once with the SFDR layer modeled as a bound asphalt layer and second time with the SFDR layer treated as an unbound granular layer. The output performance data of these models was then compared to field collected performance data to determine which approach better predicts field performance.

Many performance indicators are output in the MEPDG. In this analysis rutting was chosen for the following reasons: MnDOT regularly collects rutting data from MnROAD cells, there was no reported cracking in cells 2, 3, and 4, and no IDT creep and strength data was available for these three cells.

The six models were built in the MEPDG and run for a design life of 20 years. Since the three MnROAD cells were constructed six years ago and field data was available for 5 years, only the first five years of predictions were used for this analysis. Plots of the total rutting versus the pavement age were created for each of the three cells. The rutting predictions from MEPDG are shown in Fig. 3.2, 3.3, and 3.4. The measured total rutting, the MEPDG total rutting output for modeling the SFDR as a bound asphalt layer, and the MEPDG total rutting output for modeling the SFDR as an unbound granular layer were plotted on the same graphs for easy comparison.

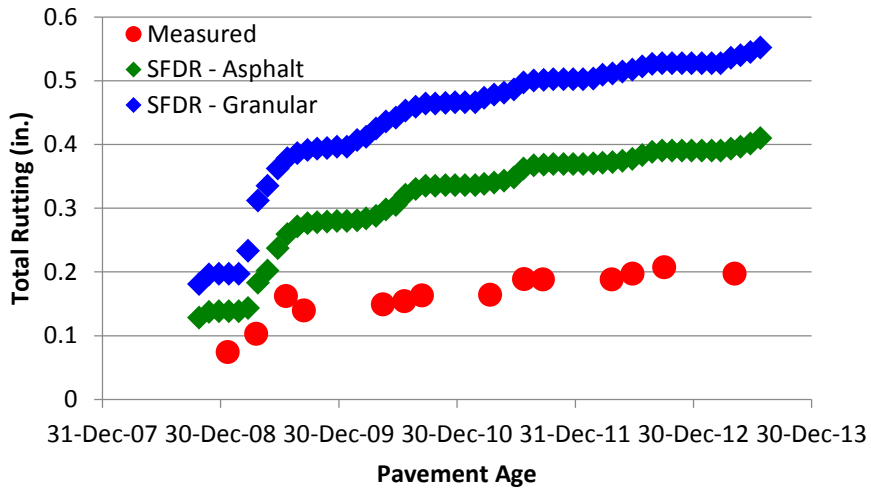


Figure 3.2: Comparison of total rutting for MnROAD cell 2

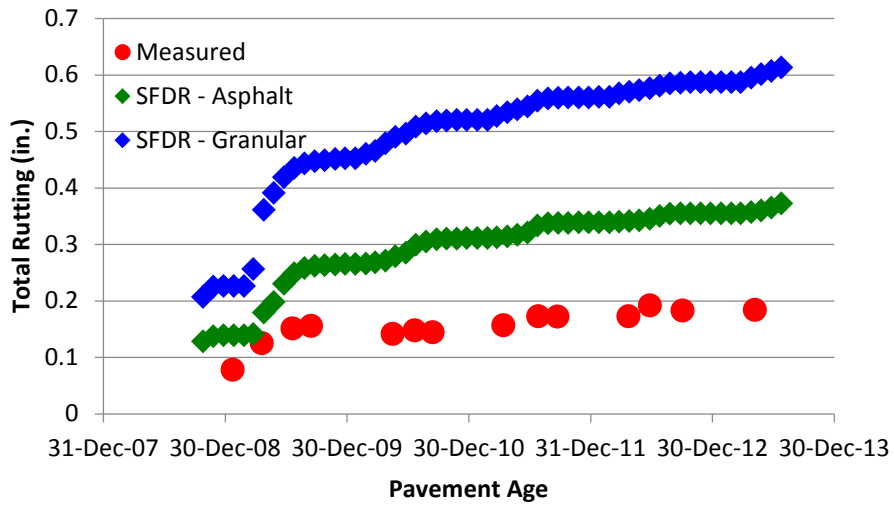


Figure 3.3: Comparison of total rutting for MnROAD cell 3

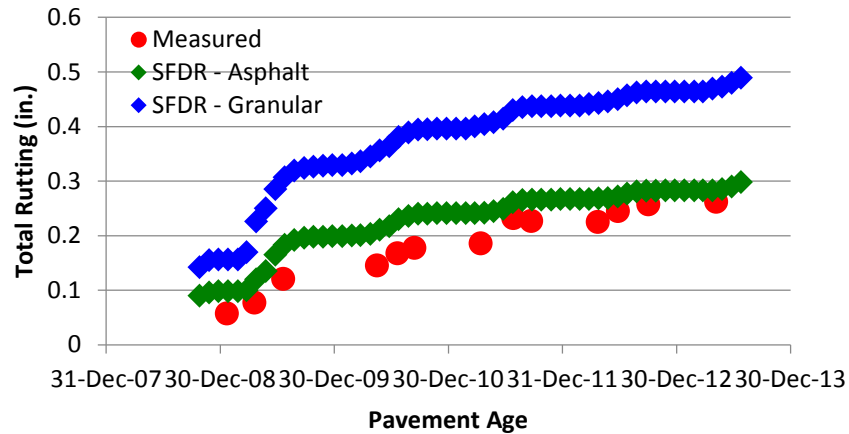


Figure 3.4: Comparison of total rutting for MnROAD cell 4

To better compare the results of the MEPDG simulations with the measured rutting values, Table 3.6 reports the MEPDG total rutting values as well as the measured total rutting values for the most current data point, May 7, 2013. A percent difference is reported for the difference between the MEPDG output and the measured field value for total rutting.

Table 3.6: Comparison of MEPDG models with measured total rutting values for 05/07/2013

Cell 2			
Model Type	Measured Rutting (in.)	MEPDG Rutting (in.)	% Difference
Bound Asphalt	0.1971	0.3960	101 %
Unbound Granular	0.1971	0.5400	174 %
Cell 3			
Model Type	Measured Rutting (in.)	MEPDG Rutting (in.)	% Difference
Bound Asphalt	0.1837	0.3600	96.0 %
Unbound Granular	0.1837	0.6010	227 %
Cell 4			
Model Type	Measured Rutting (in.)	MEPDG Rutting (in.)	% Difference
Bound Asphalt	0.2620	0.2850	8.78 %
Unbound Granular	0.2620	0.4730	80.5 %

For all three cells, the smallest difference between the predicted and the measured rutting was observed for the case when the SFDR material was modeled as a bound asphalt layer rather than an unbound granular layer. For cell 4 in particular, the prediction was very close to the measured permanent deformation.

One potential difficulty of modeling the SFDR material as a bound asphalt layer is that it requires the determination of the binder complex shear modulus $|G^*|$. This could lead to difficulty when modeling SFDR materials that have not been stabilized with an asphalt emulsion, but rather some other type of stabilizer such as cement, lime, fly ash, etc. A sensitivity analysis was performed for $|G^*|$. By varying $|G^*|$ by a factor of 500 and fixing all other input parameters, only an 11% variation was observed in the total rutting output by the MEPDG over a design life of 20 years. This result is expected because the level 1 (or 2) binder complex modulus and phase angle data are required for the global aging model and the primary input in the analysis is the asphalt concrete complex modulus $|E^*|$. The results of the sensitivity analysis are provided in Appendix A.

3.4 Summary

Based on the analysis performed in this task, it was determined that the best method for modeling SFDR layer in the MEPDG is to consider it as a bound asphalt layer. This approach requires the determination of the material's complex modulus $|E^*|$. Therefore, $|E^*|$ laboratory tests were performed on the SFDR cores for this research project.

CHAPTER 4: MATERIAL TESTING

Asphalt material tests were performed on SFDR samples provided by MnDOT to determine material properties for use in the later MEDPG simulations. Indirect tensile (IDT), dynamic modulus, and semi-circular bending (SCB) tests were performed at the University of Minnesota to determine creep compliance, tensile strength, Poisson’s ratio, dynamic modulus and fracture energy. Disc-shaped compact tension (DCT) tests were performed by MnDOT as a second measure of fracture energy.

4.1 Specimen Preparation

Cores were taken by MnDOT from sections of state highway where different types of SFDR were used. The stabilizing agents include engineered emulsion, foamed asphalt with cement, and CSS-1 with cement. Approximately 20 specimens were cored from each site. The quality of the cores varied between sites. Some sites did not have an adequate number of samples in good enough condition to test. It was determined that a total of four sites from two highways (Table 4.1) could be tested. Eight or nine specimens from each of the sites were collected for testing at the University of Minnesota. Other specimens were to be tested by the MnDOT Materials Office. The specimen labels assigned by MnDOT are used throughout this report. The number refers to the highway where the core was taken. The first letter refers to the stabilizing agent used in the SFDR (C=CSS-1 with cement, F=foamed asphalt with cement, E=engineered emulsion). The second letter designates the individual specimen.

Table 4.1: Specimens used for testing

Site	SFDR Type		Specimen Label	Number of Specimens Tested	Core Location
TH 55	CSS-1 with Cement		TH55-C	9	0.2 miles west of RP 49
TH 55	Foamed Asphalt with Cement		TH55-F	8	0.6 miles west of RP 51
TH 65	CSS-1 with Cement		TH65-C	9	0.2 miles north of RP 71
TH 65	Engineered Emulsion		TH65-E	9	0.2 miles north of RP 76

All of the specimens are from north-central Minnesota. The TH 55 sites are near Kensington, Minnesota. The TH 65 sites area sites are near Mora, Minnesota. Both highways are classified as rural arterial roads.

Cores were approximately 150 millimeters in diameter and consisted of one layer of hot mix asphalt and two layers of SFDR. Some of the cores only had one layer of SFDR intact. Only the layer of SFDR closest to the asphalt was used in testing.

4.2 IDT Test – Creep Compliance

Creep compliance is a measure of time-dependent strain divided by the applied stress. Creep compliance was determined using the IDT test in accordance with AASHTO T322-03 [35]. Specimens were tested in a temperature controlled indirect tensile test system under a constant diametrical compression load (Fig. 4.1). Testing took place in an environmental chamber at -18°C .



Figure 4.1: SFDR specimen in IDT creep test

Three specimens were tested for each site. Trimmed means for each site were used for analysis as recommended by AASHTO T322. In the cases of TH55-C and TH65-C, only two tests were successful so the data from the two tests was averaged. Average creep compliances for each site are shown in Table 4.2. Results for individual specimens are shown in Table B.1 and Table B.2 in Appendix B.

Table 4.2: Creep compliance (GPa^{-1})

Time of Loading (s)	TH55-C	TH55-F	TH65-C	TH65-E
1	0.3585	0.4825	0.2107	0.1095
2	0.3871	0.5563	0.2360	0.1396
5	0.4095	0.6290	0.2505	0.1531
10	0.4244	0.6764	0.2667	0.1590
20	0.4282	0.7348	0.2839	0.1690
50	0.4580	0.8691	0.3011	0.1761
100	0.5116	0.9727	0.3364	0.1684

It is seen that the engineered emulsion specimens (TH65-E) had the lowest creep compliance followed by the CSS-1 with cement specimens (TH55-C and TH65-C). The foamed asphalt with cement (TH55-F) had the highest creep compliance.

Poisson's ratios were also calculated from the IDT creep test. The average Poisson's ratios using trimmed means are listed in Table 4.3. Poisson's ratios for each individual specimen are shown in Table B.3 and Table B.4 in Appendix B. The results show a similar trend to the creep compliance results with the engineered emulsion having the lowest Poisson's ratio and the foamed asphalt with cement having the highest.

Table 4.3: Poisson's ratio calculated from IDT creep test

Time of Loading (s)	TH55-C	TH55-F	TH65-C	TH65-E
1	0.359	0.441	0.203	0.145
2	0.378	0.347	0.193	0.110
5	0.376	0.362	0.191	0.134
10	0.378	0.365	0.205	0.137
20	0.330	0.370	0.224	0.146
50	0.337	0.442	0.226	0.141
100	0.420	0.464	0.299	0.092

4.3 IDT Strength Test

Tensile strength was calculated following the AASHTO T322 procedure for fatigue cracking with the same specimens used for the IDT creep tests. Specimens were loaded with a constant displacement using the same apparatus as used in the IDT creep tests. Tests were conducted at -18°C . The maximum load was used to calculate the strength of each specimen using the formula from AASHTO T322. The average strength for each site is shown in Table 4.4. The tensile strengths for each individual specimen are shown Table B.5 of Appendix B.

Table 4.4: Tensile strength

Site	Tensile Strength
55-C	0.320 MPa
55-F	0.195 MPa
65-C	0.355 MPa
65-E	0.961 MPa

The engineered emulsion specimens have almost three times the tensile strength of the CSS-1 with cement specimens. The specimens made of foamed asphalt with cement have the lowest tensile strengths. It is seen that the tensile strength has negative correlation with creep compliance and Poisson's ratio.

4.4 Dynamic Modulus

Dynamic modulus, also known as complex modulus, is a measure of the maximum stress related to the maximum strain for viscoelastic materials. Typically the dynamic modulus is measured in compression on cylinders 100 mm in diameter and 170 mm tall [36]. However, the specimens obtained from the coring were approximately 150 mm in diameter and 50 mm tall so it would not

be possible to perform dynamic modulus testing using the traditional procedure. Instead, testing was performed in IDT mode following a method recently developed by Kim et al. [37].

Each specimen was loaded sinusoidally at three temperatures (-10 ° C, +10 ° C and 35 ° C) and at eight frequencies ranging from 25 Hz to 0.01 Hz. This selection of temperatures and frequencies was suggested by Kim et al. [37] as an alternative to the temperatures and frequencies recommended by the MEPDG guide [38] because it reduces the time required for specimen cooling, allowing one entire dynamic modulus test to be able to be performed in one working day.

The dynamic modulus was computed following Kim et al. [37]. First, four integrals were computed based on the geometry of the specimens:

$$F = \int_{-l}^l \frac{(1 - x^2/R^2)\sin 2\alpha}{1 + 2\left(\frac{x^2}{R^2}\right)\cos 2\alpha + x^4/R^4} dx \quad (4-1)$$

$$G = \int_{-l}^l \tan^{-1} \left[\frac{1 - x^2/R^2}{1 + x^2/R^2} \tan \alpha \right] dx \quad (4-2)$$

$$M = \int_{-l}^l \frac{(1 - y^2/R^2)\sin 2\alpha}{1 + 2\left(\frac{y^2}{R^2}\right)\cos 2\alpha + y^4/R^4} dy \quad (4-3)$$

$$N = \int_{-l}^l \tan^{-1} \left[\frac{1 + y^2/R^2}{1 - y^2/R^2} \tan \alpha \right] dy \quad (4-4)$$

where x and y are along the x and y axes of the specimen, respectively, and

R = radius of specimen

a = width of load

d = thickness of specimen

l = half of gauge length

α = radial angle of loading = $\sin^{-1} \left(\frac{a/2}{R} \right)$

Next, the dynamic modulus ($|E^*|$) and Poisson's ratio (ν) were computed for each of the 24 temperature and frequency combinations for each of the specimens using Eqs. 4-5 and 4-6.

$$|E^*| = 2 \frac{P_0}{\pi a d} \frac{\beta_1 U_0 - \gamma_1 V_0}{-\beta_2 U_0 + \gamma_2 V_0} \quad (4-5)$$

$$\nu = \frac{\beta_1 U_0 - \gamma_1 V_0}{-\beta_2 U_0 + \gamma_2 V_0} \quad (4-6)$$

where

P_0 = amplitude of applied load

U_0 = amplitude of horizontal displacement (averaged between the two sides)

V_0 = amplitude of vertical displacement (averaged between the two sides)

Where P_0 , U_0 , and V_0 were taken as half of the distance between the smallest and largest values for the last five cycles of loading, and

$$\beta_1 = -N - M \quad (4-7)$$

$$\beta_2 = N - M \quad (4-8)$$

$$\gamma_1 = F - G \quad (4-9)$$

$$\gamma_2 = F + G \quad (4-10)$$

The dynamic modulus values for each specimen at each temperature and frequency are shown in Tables B.6 through B.8 in Appendix B. Note that some values are missing because some of tests were not able to be completed at the highest temperatures and frequencies.

The dynamic modulus data for each specimen was fit to master curves using Witczak's sigmoid, as described by Rowe, et al. [39]. The MEPDG guide [38] uses a similar approach. Master curves were created at a reference temperature of +10 ° C by fitting the data to Eq. 4-11:

$$\log|E^*| = \delta + \frac{\alpha - \delta}{1 + e^{\beta + \gamma(\log \omega + \log(a(T)))}} \quad (4-11)$$

where ω is the frequency of the load, $a(T)$ is the parameter for the temperature shift, δ , α , β and γ are fitting parameters.

Dynamic modulus master curves are traditionally plotted against reduced frequency, which can be calculated as follows:

$$\text{Reduced Frequency} = 10^{\log \omega + \log a(T)} \quad (4-12)$$

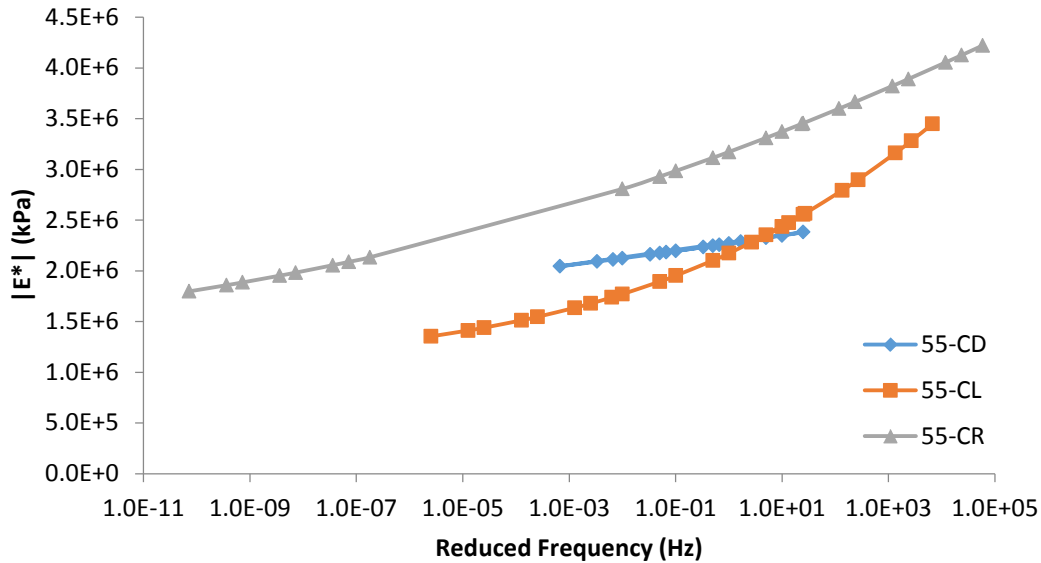


Figure 4.2: Dynamic modulus master curve for TH55-C specimens

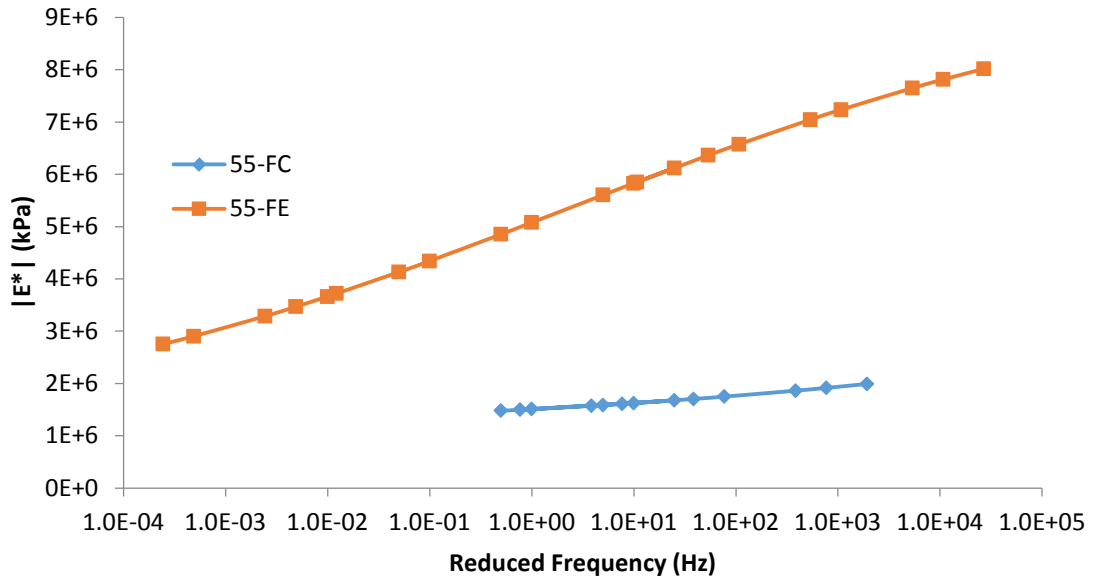


Figure 4.3: Dynamic modulus master curve for TH55-F specimens

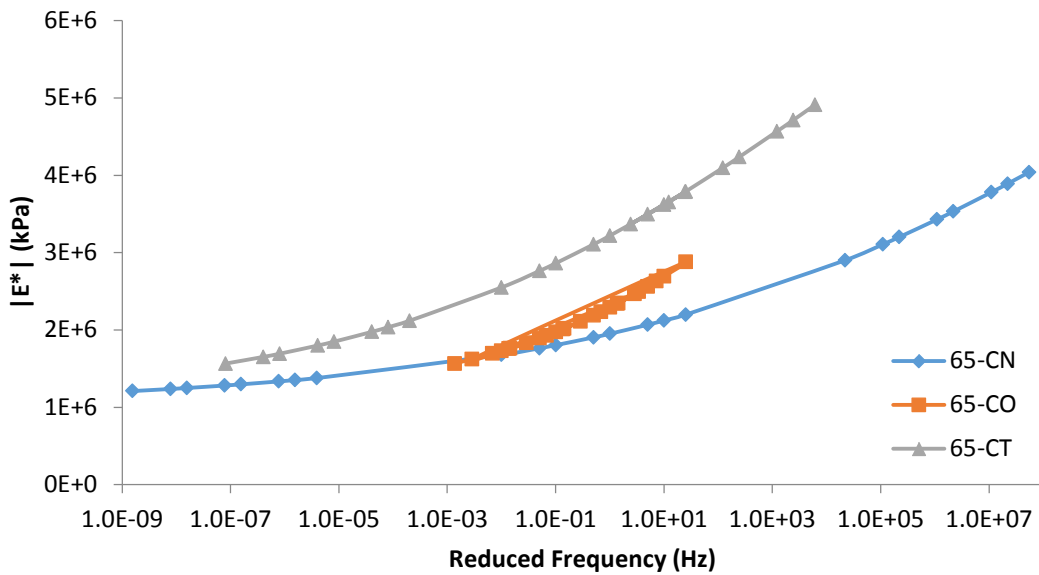


Figure 4.4: Dynamic modulus master curve for TH65-C specimens

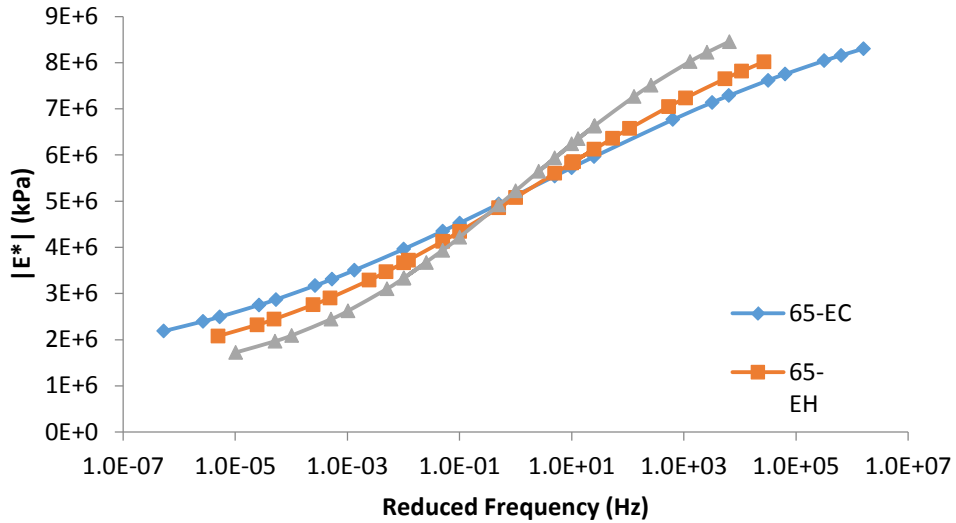


Figure 4.5: Dynamic modulus master curve for TH65-E specimens

Figs. 4.2 through 4.5 show that the TH65-E specimens have the highest dynamic moduli and the most cohesive master curves. Some of the test results for the other specimens were inconsistent, which created difficulties in fitting the master curves.

4.5 Semi-Circular Bending Test

Semi-circular bending (SCB) tests were conducted to determine fracture energy. Testing was performed according to the AASHTO Standard Method of Test for Determining the Fracture Energy of Asphalt Mixtures Using the Semi Circular Bend Geometry [40]. Specimens were cut in half into semicircles. Both halves of each specimen were tested when possible. Specimens labels (1) and (2) refer to the two semicircular specimens cut from one original cylindrical specimen. A vertical crack was cut in each semicircular specimen. Specimens were instrumented to monitor the crack opening while being loaded vertically (Fig. 4.6).



Figure 4.6: SCB test set-up

In this research, a MTS servo-hydraulic testing system equipped with an environmental chamber was used to perform the SCB test. The SCB samples were symmetrically supported by two fixed rollers and had a span of 120 mm. The load line displacement (LLD) was measured using a

vertically mounted Epsilon extensometer with 38 mm gage length and ± 1 mm range; one end was mounted on a button that was permanently fixed on a specially made frame, and the other end was attached to a metal button glued to the sample. The crack mouth opening displacement (CMOD) was recorded by an Epsilon clip gage with 10 mm gage length and a +2.5 and -1 mm range. The clip gage was attached at the bottom of the specimen. Considering the brittle behavior of asphalt mixtures at low temperatures, the CMOD signal was used as the control signal to maintain the test stability in the post-peak region of the test. Plots of the crack opening versus the load are shown in Figs. 4.7 through 4.10. The number of specimens successfully tested was smaller than preferred due to problems keeping the crack gauges connected to the specimens.

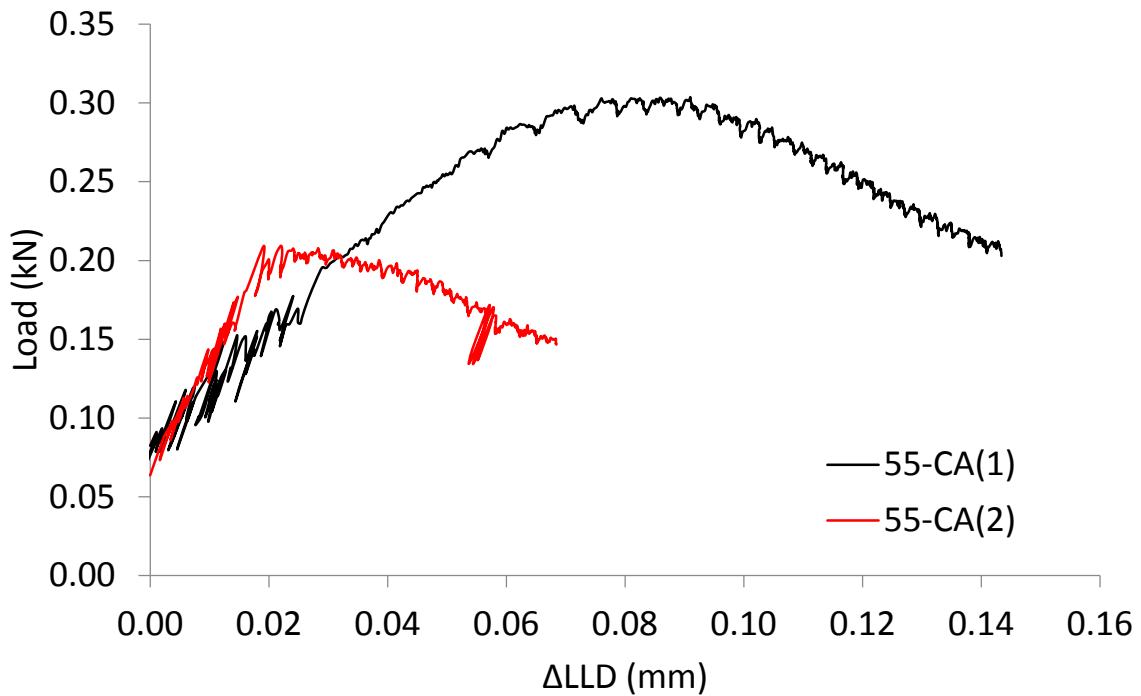


Figure 4.7: SCB Load versus crack opening TH55-C

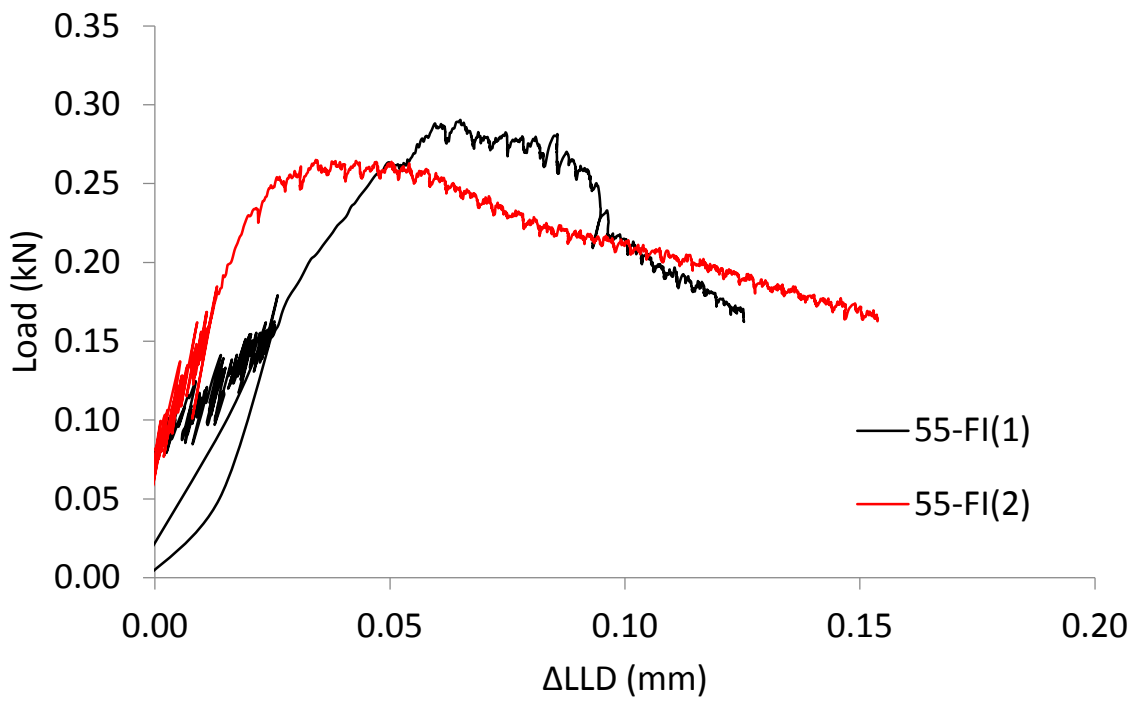


Figure 4.8: SCB Load versus crack opening TH55-F

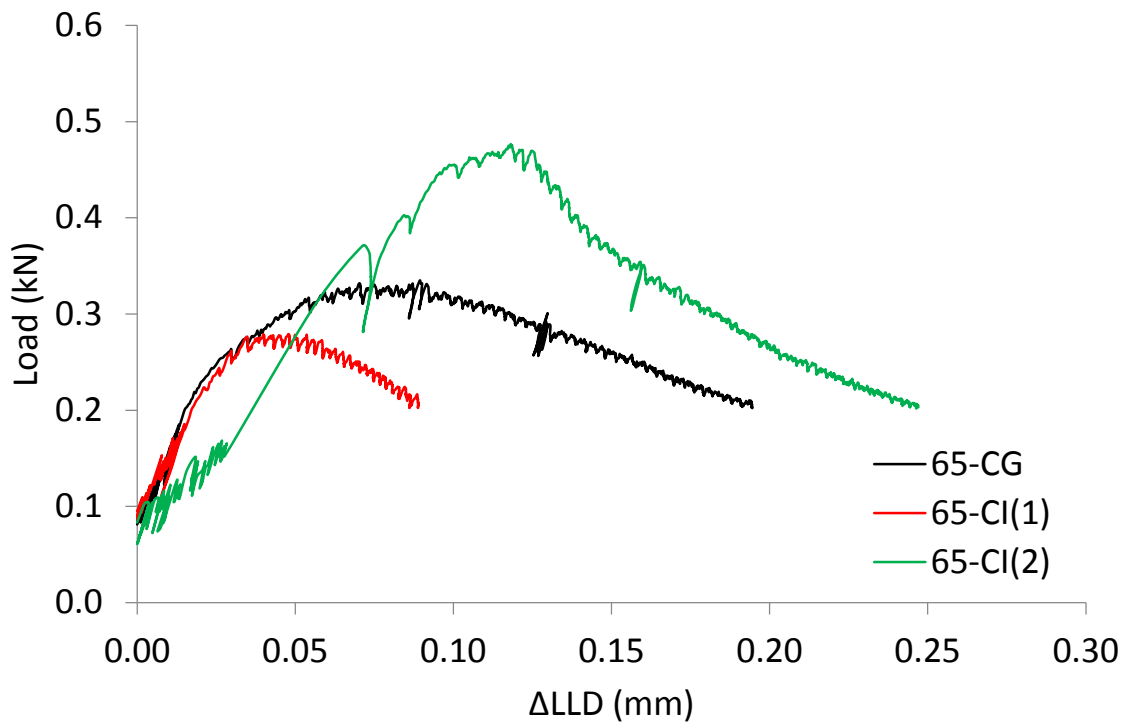


Figure 4.9: SCB Load versus crack opening TH65-C

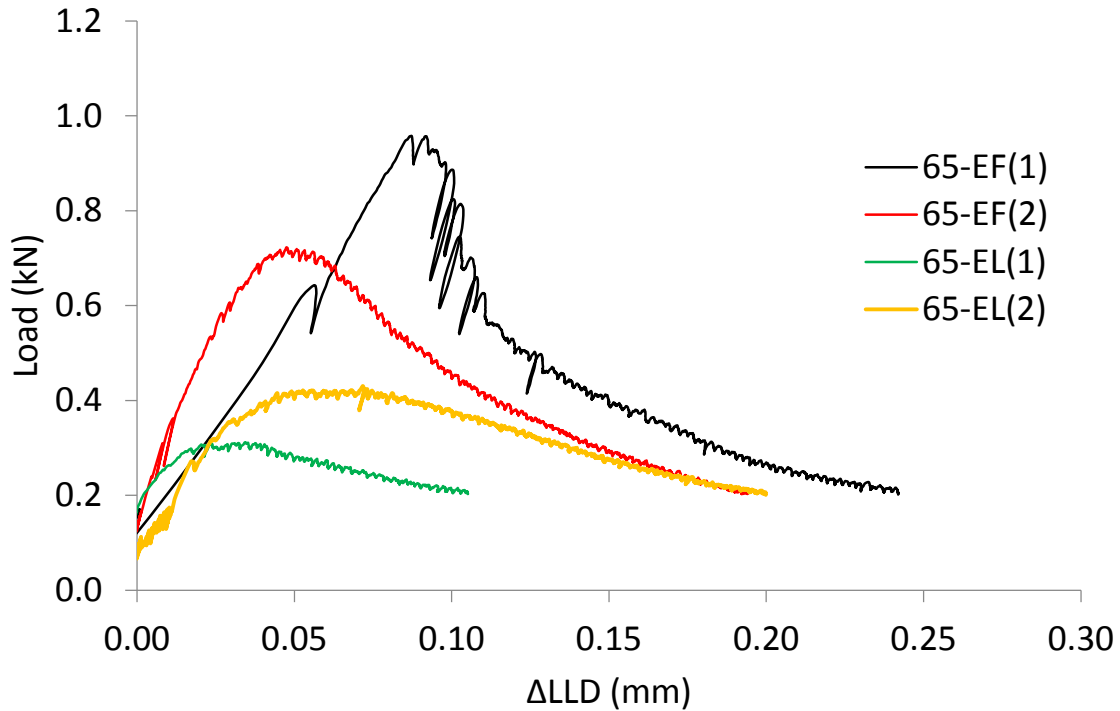


Figure 4.10: SCB Load versus crack opening TH65-E

The fracture energy G_f was calculated according to RILEM TC 50-FMC specification that has been extensively used in the study of concrete. The work of fracture is determined as the area under the loading-deflection ($P-u$) curve. The fracture energy G_f can then be obtained by dividing the work of fracture with the ligament area:

$$G_f = \frac{\int P du}{A_l} \quad (4-13)$$

where $\int P du$ = total work done by the external force P and A_l = ligament area. Eq. 4-13 is written based on the assumption that the external work is all spent in crack propagation and the rest of the specimen behaves elastically. This assumption is reasonable for asphalt mixture specimens at low temperatures, which generally exhibit a damage localization mechanism [41, 42].

As it can be seen from Figs. 4.7-4.10, the main difficulty using this approach is that it is next to impossible to capture the tail part of the load-deflection curve due to fact that as the crack propagates close to the top surface of the specimen, the CMOD opening typically exceeds the allowable gauge measurement limit and the test is terminated. Since the load capacity of SFDR is much lower than conventional asphalt mixtures, the minimum load limits set in the test procedure to protect the gauges stopped the testing before the full post-peak was reached so fracture energy cannot be calculated directly. This means that the work-of-fracture method cannot directly be applied to determine the fracture energy.

The so-called apparent fracture toughness can be computed from the measured peak load of the specimen within the framework of linear elastic fracture mechanics (LEFM). The essential failure criterion of LEFM is that the stress intensity factor (SIF) of the specimen reaches a critical value (i.e. fracture toughness) as the peak load is attained. The SIF of the SCB specimen can be written as [43, 44]:

$$K = \frac{P}{2rt} \sqrt{\pi a} \left\{ 4.782 + 1.219 \left(\frac{a}{r} \right) + 0.063 \exp \left[7.045 \left(\frac{a}{r} \right) \right] \right\} \quad (4-14)$$

where r = radius of the SCB specimen, t = thickness of specimen, and a = notch depth. Considering the LEFM failure criterion, we can compute the fracture toughness K_{Ic} based on Eq. 4-14 and the experimentally measured peak load. It should be emphasized here that the fracture toughness computed by the above equation is strictly anchored by the assumption of LEFM. For SCB specimen, it may be reasonably expected that the LEFM limit can be approximately reached since the size of the material inhomogenities is much less than the size of the SFDR specimens. Therefore, we can equate the apparent fracture toughness to the actual fracture toughness of the material. From the fracture toughness, the fracture energy can be calculated from the well-known Irwin's relationship:

$$G_f = K_{Ic}^2 / E \quad (4-15)$$

The elastic modulus of the material was determined from the initial slope of the measured load-deflection curve of SCB specimens. To this end, we considered the elastic modulus of the material to be equal to 1 N/m^2 , and performed an elastic finite element model to compute the stiffness: $S_0 = 0.11 \text{ N/m}$, which measures the slope of the simulated load-deflection curve (Fig. 4.11).

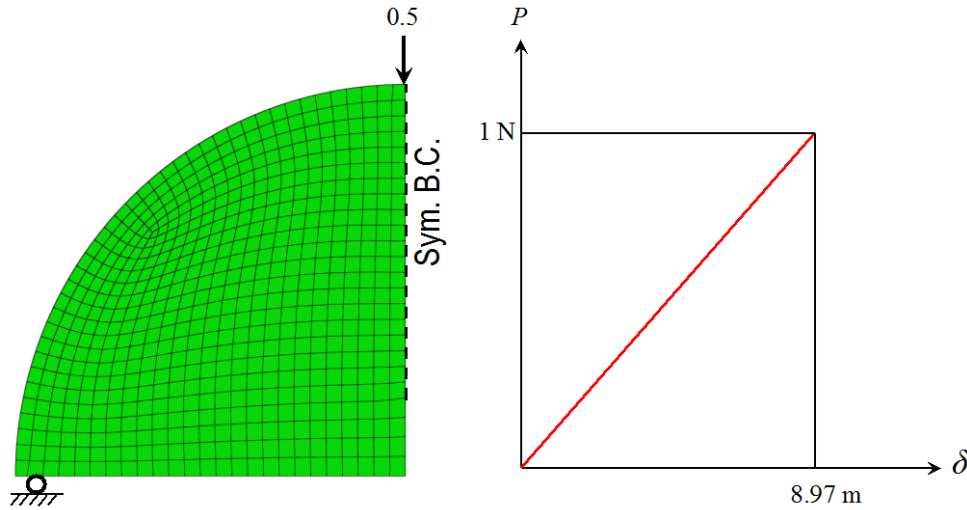


Figure 4.11: Elastic analysis of SCB specimen

The actual elastic modulus of the SFDR material can be determined as

$$E = S / S_0 \times 10^{-9} \text{ (GPa)} \quad (4-15)$$

With Eq. 4-15, we can calculate the fracture energy G_f for all four SFDR materials. The detailed values of E , K_{IC} , and G_f are listed in Table 4.5.

Table 4.5: SCB Fracture Energy Values

Specimen	S (KN/mm)	E (GPa)	K_{IC}	G_f (J/m ²)
55-CA(1)	3.519	0.0320	0.00229	164.6
55-CA(2)	7.895	0.0718	0.00158	34.8
55-FI(1)	3.75	0.0341	0.00219	141.2
55-FI(2)	8	0.0727	0.00200	55.2
65-CG	6	0.0545	0.00253	117.3
65-CI(1)	6	0.0545	0.00211	81.6
65-CI(2)	4.429	0.0403	0.00360	322.1
65-EF(1)	9.6	0.0873	0.00723	599.8
65-EF(2)	14	0.1273	0.00546	234.2
65-EL(1)	7.5	0.0682	0.00236	81.5
65-EL(2)	10.36	0.0942	0.00325	112.4

It can be seen that for each site the calculated fracture energy exhibits a large variation. This is because that the variation of the calculated fracture energy can be considered as a combined effect of the variations in both fracture toughness (or equivalently the peak load in SCB test) and the elastic modulus (or equivalently the elastic stiffness measured in SCB test). As seen, both these quantities exhibit a significant variation due to a limited number of available samples available. Therefore, the present test results should not be used for determining the statistical variation of the SFDR properties. Meanwhile, the direct compaction tension (DCT) test performed by the MnDOT materials office showed that one could obtain a fairly large portion of the post-peak behavior of the load-deflection curve and therefore the fracture energy can be directly calculated by using the work-of-fracture method. It was shown that the calculated fracture energy exhibited a much smaller variation compared to the current calculation. Therefore, we may conclude that for evaluating the fracture energy of SFDR the DCT test may yield a more consistent result compared to SCB test since it is able to reach the tail part of load-deflection curve.

4.6 Disc-Shaped Compact Tension Tests

Disc-shaped compact tension (DCT) tests were conducted by MnDOT at the MnDOT Maplewood Testing Laboratory. Specimens were prepared according to the MnDOT sample preparation procedure. Two one-inch holes and a notch were cut and drilled into each specimen following the template shown in Fig.4.12. The TH 55 specimens broke during the preparation process and were not able to be tested.



Figure 4.12: DCT Template

Testing was performed according to the MnDOT modified testing procedure using the MnDOT DCT device. Testing was performed at -18°C. The DCT fracture energy results are shown in Table 4.6. Only results for the first layer of SFDR are shown to be consistent with the other tests, which were performed only on the first layer. Full testing results for TH 65 as well as TH 56 (not otherwise included in this project) are shown in Table B.9 in Appendix B.

Table 4.6: DCT Fracture Energy Values

Specimen	Fracture Energy (J/m ²)
65-CR	14.58
65-EA	46.63
65-EE	59.35
65-EP	62.29

Table 4.7 compares fracture energy values from the SCB and DCT tests. The values are averaged over each specimen tested for each site. The SCB fracture energy values are several times larger than the DCT values. This is due to differences in testing methods, most notably the rate of loading. Nonetheless, the results from both tests show that the 65-E specimens have a higher fracture energy compared to the 65-C specimens.

Table 4.7: Fracture Energy Comparison

Site	SCB G_f (J/m ²)	DCT G_f (J/m ²)
65-C	173.67	14.58
65-E	256.98	60.82

4.7 Summary

Creep compliance, Poisson’s ratio and tensile strength were determined for each of the four sites using indirect tension (IDT) testing. It was shown that dynamic modulus could be measured through a IDT test set-up with a simple elastic stress analysis. This is essential for SFDR since the cores usually do not have a dimension that is suitable for preparation of the cylindrical specimens for conventional dynamic modulus tests. The proposed dynamic modulus tests appeared to be successful for the TH65-E specimens, but the results are questionable for the TH55-C, TH65-C and TH55-F specimens based on the observed large variation. The fracture energies of the four SFDR materials were measured by the SCB tests. Large variation is also present in the fracture energies, which is mainly due to the fact that the test is unable to reach the tail part of the load-deflection curve. Fracture energy was also measured by the DCT tests with

results significantly lower than those from SCB. Despite the difficulties with some of the tests, it is evident that the engineered emulsion SFDR specimens (TH65-E) performed best overall, with the lowest creep compliance and Poisson's ratio, the highest tensile strength, the highest dynamic modulus and the highest fracture energy.

CHAPTER 5: NUMERICAL MODELING OF SFDR BY MEPDG

Pavement structures were numerically modeled in MEPDG, using the mechanical properties determined during material testing along with information from MnDOT design documents. The modeling approach followed the recommendations described in Chapter 3 of this report, in which the SFDR layer was treated as a bound asphalt concrete layer.

Modeling was attempted for all four highway sites. However, only the TH 55 CSS-1 with cement site (TH55-C) was successfully simulated. The dynamic modulus tests on the TH 55 Foamed Asphalt with Cement (TH55-F) were incomplete due to the material specimens failing during the tests at 35°C. Without sufficient dynamic modulus results, TH55-F could not be modeled. Modeling was attempted for TH 65 CSS-1 with cement and TH 65 Engineered Emulsion but MEPDG was unable to complete the simulations. The problem was isolated to the dynamic modulus inputs.

5.1 Modeling Methodology

The TH55-C pavement was modeled in MEPDG using the methodology suggested in Chapter 3. In MEPDG, the level of detail can be selected for most parameters, where level 1 is the most detailed input and level 3 is the least detailed.

The MnDOT design memo did not specify a construction date for the section of highway where the TH55-C cores were taken. However, the letting date for the project was listed as October 2009 in the design memo so it was assumed that the construction took place in the summer of 2010. June 2010 was chosen as the date of construction and traffic opening.

Traffic data was input using level 3. For the TH55-C simulations, an AADTT of 90 and a linear growth rate of 1.1% were used, as specified in the MnDOT design memo. The default MEPDG values were used for monthly adjustment, hourly distribution and vehicle class distribution. The speed limit was not specified in the MnDOT design memo so 55 miles per hour, the typical speed limit for Minnesota state highways [45], was used.

5.2 Pavement Structure

Pavement structure information was taken from the MnDOT design memo. The structure for the TH55-C core was modeled with five inches of asphalt, eight inches of SFDR and a six inch base, as shown below in Fig. 5.1.

5" PG 58-34 Asphalt
8" SFDR
6" Base
Subgrade

Figure 5.1: TH55-C Pavement Structure

The SFDR layer was modeled as a flexible pavement (asphalt) with level 1 inputs using the material testing results in Chapter 4. All of the other materials were modeled with level 3 with the default inputs for each material type because of the lack of detailed information.

The asphalt was modeled as a single 5” layer of PG 58-34 asphalt. The design memo states that 3 lifts of asphalt were used for a total of 5”. The asphalt cement test report states that the asphalt used meets the requirements of PG 58-34.

For the SFDR layer, dynamic modulus data from Chapter 4 was used. The data required manipulation to fit MEPDG’s input format. This manipulation is discussed in section 5.3. Level 1 inputs also require asphalt binder test data. Binder tests were not performed during the material testing so the binder data used in the test simulations in Chapter 3 was used. The data is shown in Table 5.1. This binder data is for engineered emulsion; however, simulations in section 3 showed that rutting results were not sensitive to the binder test data. An additional sensitivity analysis specific to the TH55-C data was performed and is described in section 5.4 of this report. A Poisson’s ratio of 0.35 was used for the simulation rather than the 0.42 experimental value from the materials testing because 0.42 was believed to be high. A simulation using a Poisson’s ratio 0.42 was also conducted. Results for that simulation are in section 5.4.

Table 5.1: G^* Binder Test Data Inputs

Temperature (°F)	G^* (Pa)	Phase Angle (°)
104	4473	84.4
114.8	2398	85.8
125.6	1073	87.3

The base was modeled as a 6” layer of A-1-a. AASHTO soil classification A-1-a is described as granular material consisting of mainly stone fragments, gravel and sand [46]. The design memo describes the base as sand and gravel. The subgrade was modeled as an infinite layer of A-4, described as silty soil in the AASHTO soil classification system [46]. The design memo describes the subgrade as silt loam (SiL) with an R-value of 27.6. The MnDOT Pavement Design manual States that SiL soil corresponds to A-4 AASHTO soil classification [47].

Table 5.2: Creep Compliance Data Inputs

Loading Time (sec)	Creep Compliance (1/psi)
1	0.359
2	0.378
5	0.376
10	0.378
20	0.33
50	0.337
100	0.42

Thermal cracking was input using level 2 because levels 1 and 3 both require creep compliance test data at multiple temperatures, while level 2 requires testing at a single temperature. For level

2, creep compliance data is should be at 14°F; however, creep compliance testing was conducted at -18 ° C (-0.4° F). The creep compliance data entered is shown in Table 5.2. It is believed that the temperature difference will have little impact on the results. Thermal cracking analysis also requires tensile strength. The average tensile strength was taken from the IDT tensile strength test as 46.4 psi.

5.3 Dynamic Modulus Data Temperature Shifting

Dynamic modulus tests were performed at 3 temperatures (-10° C, +10° C, and +35° C) and 8 frequencies ranging from 25 Hz to 0.01 Hz as suggested by Kim, et al. [37]. This procedure was developed to save time over the AASHTO procedure [36], which requires specimens to be tested at five temperatures and six frequencies. MEPDG requires data at a minimum of four temperatures, including between 125 ° F and 135 ° F (52 ° C and 57 ° C) and between 60 ° F and 90° F (15 ° C and 32° C).

The method to create an input table for MEPDG is similar to that used in section 4.4 to create master curves. First, the values of dynamic modulus for each temperature and frequency were averaged over the three TH55-C specimens. Then, using optimization in Microsoft Excel, the values were fit to Eq. 5-1 [39].

$$\log|E^*| = \delta + \frac{(m - \delta)}{1 + e^{\beta + \gamma(\log t_r)}} \quad (5-1)$$

where

- $\log(t_r) = \log(\omega_r) - \log(a(T))$
- $\omega_r =$ testing frequency
- $a(T) =$ shift factor to new frequency
- $m, \delta, \beta, \gamma =$ fitting parameters

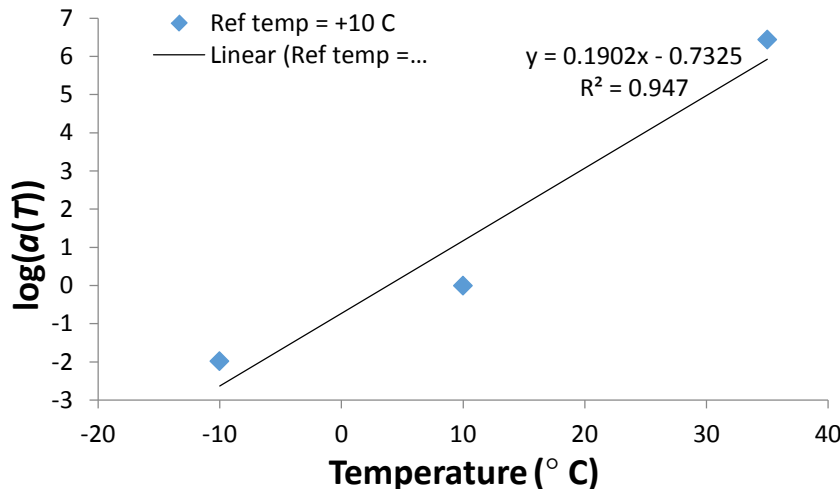


Figure 5.2: Temperature shift factor $\log(a(T))$ plotted against temperature and its fit by a linear function

The fitted E^* could be plotted against $\log(t_r)$ to form the master curve at $+10^\circ\text{C}$. The $\log(a(T))$ values obtained from the curve fitting form a linear relationship when plotted against temperature, as shown in Fig. 5.2. The three data points fit the trend line with an R -squared value of 0.947. This relationship was used to find the shift factor $\log(a(T))$ at the other desired temperatures. This factor was then used in the equation to find the E^* values at the new temperatures. Finally, the E^* data was converted to psi for the use in MEPDG. The E^* values used in the MEPDG simulations are shown below in Table 5.3.

Table 5.3: TH55-C Dynamic Modulus Inputs (psi)

Temp (°F) Frequency (Hz)	25	10	5	1	0.5	0.1	0.05	0.01
14	485001.2	470027	459018.9	434479.5	424334.7	401717.1	392365.7	371515
95	251649.7	244079.8	238511.2	226086.1	220944.7	209471.2	204723	194126
68	326523.8	316596.8	309296.2	293012.7	286277.2	271252.2	265036.5	251169.8
131	195814.8	189986.4	185697.9	176125.4	172162.8	163316.8	159654.5	151478.1

5.4 MEPDG Results and Comparison to Measured Rutting

The MEPDG simulation for TH55-C with the inputs described above predicted that the maximum total rutting at three years would be 0.141 inches. In 2013 (approximately 3 years after construction) MnDOT measured the total rutting as 0.07 inches, which is about half the value predicted by MEPDG. However, a 2009 MnDOT report [48] found that MEPDG typically over predicts total rutting. The report suggests subtracting the subgrade and base rutting predicted for the first month from the total predicted rutting. Following this procedure, the total rutting at three years would be 0.864, which is still an over prediction, but much closer to the measured rutting.

5.5 Sensitivity Analysis

A number of MEPDG simulations were performed by changing one input parameter at a time in order to examine the sensitivity of changing certain variables and to attempt to get a rutting value closer to MnDOT's measured value. These tests included doubling the G^* values for the SFDR binder test, using a Poisson's ratio of 0.42 (the measured value in Chapter 4), and using the 1936, the original construction year of the road, for the base and subgrade construction date. In addition, a simulation was run using default values provided by MnDOT for the unknown parameters, which differ slightly from the MEPDG default values. The results of these simulations are shown in Table 5.4 along with the values from the first simulation. Rutting values are shown from 2.5 years to 3.5 years because the months of construction and inspection are unknown. The initial base and subgrade rutting has been subtracted as described in section 5.4

Table 5.4: Total Rutting (inches)

Year	Base Case	Double G^*	$\nu=0.42$	1936 Base Construction	MnDOT Defaults
2.5	0.0813	0.0813	0.0809	0.0795	0.0813
2.58	0.0813	0.0813	0.0811	0.0805	0.0813
2.67	0.0813	0.0813	0.0812	0.0805	0.0813
2.75	0.0813	0.0813	0.0812	0.0805	0.0813
2.83	0.0833	0.0833	0.0825	0.0815	0.0833
2.92	0.0843	0.0843	0.0841	0.0835	0.0843
3	0.0863	0.0863	0.0859	0.0845	0.0863
3.08	0.0883	0.0883	0.0875	0.0865	0.0883
3.17	0.0903	0.0903	0.0895	0.0885	0.0903
3.25	0.0913	0.0913	0.0911	0.0895	0.0913
3.33	0.0923	0.0923	0.0919	0.0905	0.0923
3.42	0.0923	0.0923	0.0923	0.0905	0.0923
3.5	0.0933	0.0933	0.0927	0.0905	0.0933

It is seen that doubling G^* showed no change in rutting, which confirms the conclusion from Chapter 3 that the binder test data has little effect on rutting. Changing the construction year of the base and subgrade also had no effect of the rutting. Using the higher Poisson's ratio and using MnDOT's default values both lowered the rutting slightly, bringing the predicted rutting values slightly closer to the measured valued. It should be emphasized that the current comparison is performed against a single field measurement. Given that the properties of SFDR materials are well expected to exhibit a spatial variability, the MEPDG result can be considered to be reasonably acceptable for rutting prediction.

5.6 Limitations of MEPDG

Several difficulties were encountered in attempting perform simulations using MEPDG. When certain values were input, MEPDG would complete the traffic, climate, and thermal cracking steps of analysis steps of the analysis but the program would always stop running before starting the (asphalt concrete) AC analysis step. This behavior was consistent for multiple attempts with the same parameters. While the TH55-C simulations were successful, simulations for TH65-C and TH65-E were not able to complete the analysis. Parameters were changed from the values for TH55-C to the values for TH65-E one at a time to find the cause of the problem. The issue was isolated to the dynamic modulus values. It is believed that dynamic modulus values that are outside of a certain range cause MEPDG to hang-up and be unable to complete the asphalt analysis, causing the program to stop responding. Due to this issue, simulations for TH65-C and TH65-E were not able to be performed.

In addition to the issue regarding the dynamic modulus values, the value of MEPDG is limited in that the program requires thirty to forty-five minutes to run a single simulation. This cost makes conducting a parametric analysis using MEPDG impractical for the limited period of this project. Therefore, other options were explored for the parametric analysis step of the study.

5.7 Summary

The numerical modeling of four SFDR projects was attempted by using the MEPDG software. It was observed that the MEPDG could yield a reasonable prediction of the rutting performance of SFDR. However, the investigation also indicated that MEPDG seems to have a required range of input dynamic modulus values, beyond which the simulation ceases. Two of these SFDR projects came across this difficulty. Therefore, even though the MEPDG could yield the complete time evolution of rutting performance, it is not guaranteed that it could be used for every SFDR project. Meanwhile, it was also noted that MEPDG requires a considerable amount of computational time, which could be prohibitive for extensive parametric studies for determining the relationship between mechanical properties of SFDR materials and their long-term rutting performance.

CHAPTER 6: NUMERICAL MODELING OF SFDR BY MNPAVE

Due to the limitations to MEPDG described in section 5.6, MnPAVE was chosen as an alternative modeling technique. MnPAVE is an asphalt pavement analysis program developed by MnDOT and specific to Minnesota. It is similar to MEPDG in that it also uses mechanics and empirical relationships, but it is a simpler program. MnPAVE runs much faster than MEPDG, generating immediate results for design life and requiring less than a minute to perform one single Monte Carlo reliability simulation in comparison to 30 to 45 minutes for one MEPDG simulation. For this research, MnPAVE version 6.3 was utilized in research mode.

6.1 Design Inputs

MnPAVE has the following four input categories: project, climate, traffic and structure.

6.1.1 Project

The project information section requires the information of MnDOT district and county. The county is used as the location for the weather data unless a more exact location is specified in the climate section.

The project information section also has fields for project number, route, city, reference post, letting date, construction type, designer, soils engineer, and notes. However, these fields are optional and for informational purposes only; they do not affect the analysis results.

6.1.2 Climate

The climate section shows a map of the state of Minnesota with the counties outlined and the MnDOT districts divided by color. The mark on the map defaults to the center of the county specified in the project information section. However, the user can change the location of the analysis either by selecting a different location on the map or by entering latitude and longitude coordinates.

MnPAVE analyzes climate using five seasons: fall (standard), winter (frozen), early spring (base thaw), late spring (soil thaw), and summer (high temperature). This is in contrast to MEPDG, where hourly climate information is used. The difference in the detail of the temperature data is one of the ways that MnPAVE saves efficiency compared to MEPDG. Based on the selected location, MnPAVE displays the number of days or weeks in each of the five seasons and the average pavement temperature for that season. There is also an option for the user to input this data manually.

6.1.3 Traffic

MnPAVE has two options for entering traffic – ESAL (equivalent single axle load) and load spectrum. In the load spectrum option, MnPAVE converts the traffic to ESALs during the analysis which significantly increases the computation time so the ESAL option was selected. For ESAL mode, MnPAVE gives the option to enter lifetime or first year ESALs in millions along with the design period length and the annual growth rate (simple or compound). From this information it calculates either the lifetime or first year ESALs (whichever was not entered). The

pavement functional type - interstate, major arterial, minor arterial, collector/local, or other – is also required. In addition, the traffic section has input fields for tire and axle information.

6.1.4 Structure

MnPAVE allows the user to input up to five layers, with the last layer being infinite. There is an SFDR option for the second layer, which was used for this research. The user can either select a subtype for each layer or input material properties directly. The user can also select the confidence level desired for the design.

6.2 MnPAVE Outputs

MnPAVE outputs pavement design life for fatigue and rutting. Rutting design life is based on a half inch limit. MnPAVE limits the design life calculation to a maximum of 50 years. MnPAVE also has option to run a Monte Carlo simulation for fatigue and rutting reliability. The reliability level is defined as the probability that the pavement will survive (have less than a half inch of rutting) for the original. Only the rutting results were studied. The user is able to select the number of Monte Carlo cycles. Two thousand five hundred cycles, the MnPAVE default, were used for all simulations in this report. There are also several other output options such as thickness goal seek and quick reliability that were not used for this research.

6.3 Modeling of 55C in MnPAVE

The TH55-C pavement structure was modeled in MnPAVE so that the results could be compared with the MEPDG results.

6.3.1 Project, Climate and Traffic Inputs

The project location was selected as Douglas County. The MnPAVE default location within the county (45° 55' N, 95° 27' W) was used for the analysis. The weather data is as shown in Table 6.1.

Table 6.1: MnPAVE climate data for TH55-C

	Fall	Winter	Early Spring	Late Spring	Summer
Temperature (° F)	49	21	38	58	81
Days	91	106	14	59	95

Traffic was input as 0.698 million lifetime ESALs with a 1.4% simple annual growth rate for a 35 year design period. The pavement functional type was classified as a minor arterial because rural minor arterial is not an option in MnPAVE. MnPAVE default values were used for the axle configuration and allowable stress failure criterion sections.

6.3.2 Structure Inputs

The pavement structure was input as shown in Fig. 6.1. The materials were selected to match the pavement design memo and MEPDG simulation for TH55-C as closely as possible. The 0” undisturbed soil layer was required for MnPAVE analysis. The default confidence level of 70 was used. Default values for each specific material from basic mode were used for the asphalt, aggregate base and soil layers. Dynamic modulus values for the SFDR layer were entered on advanced mode.

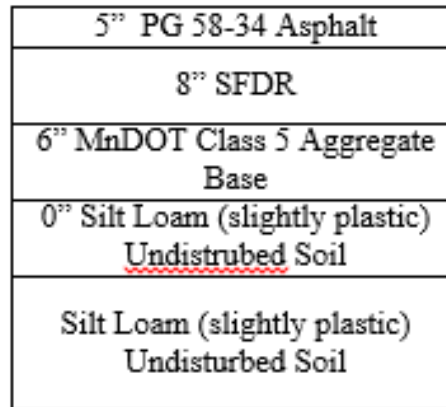


Figure 6.1: TH55-C pavement structure for MnPAVE

To input dynamic modulus values into MnPAVE in advanced mode one E^* value, corresponding to the load frequency, is required for each of the five seasons. This is in contrast to MEPDG where values for a range of temperatures and frequencies are required. To calculate the required values from the experimental dynamic modulus values found in Chapter 4 of this report the load frequency was needed. Load time was calculated from Eq. 6-1, developed by Brown [49, 50].

$$\log t = 0.5 \log d - 0.2 - 0.94 \log v \tag{6-1}$$

where

- t = loading time (seconds)
- d = pavement depth (meters)
- v = vehicle speed (kilometers/hour).

Pavement depth was taken as the combined depth of the asphalt and SFDR, a total of 13” for TH55-C. As in the MEPDG analysis in Chapter 5, a design speed of 55 miles per hour was assumed. Using Eq. 6-1 the load time was calculated as 0.01364 seconds. Frequency was calculated as

$$f = \frac{1}{2\pi t} \quad (6-2)$$

where t is the loading time in seconds and f is the frequency in hertz. Eq. 6-2 gives a loading frequency of 11.67 Hz for TH55-C. The relationship expressed in Eq. 6-2 has been suggested by several sources [50, 51]. It was chosen over the traditional $f=1/t$ relationship between frequency and period because it gave a more reasonable result for loading frequency (11.67 Hz versus 73.29 Hz).

To determine the dynamic modulus values for 11.67 Hz frequency, the $\log(a(T))$ temperature shift factors were found for each of the five seasonal temperatures in Table 6.1 using the procedure described in section 5.3. The dynamic modulus values for those temperatures were calculated with Eq. 5-1 and are shown in Table 6.2.

Table 6.2: 55C Dynamic Modulus Values for MnPAVE

	Fall	Winter	Early Spring	Late Spring	Summer
E^* (ksi)	372.04	473.09	407.44	342.64	286.15

6.3.3 Results and Comparison to MEPDG

The MnPAVE prediction for TH55-C was a design life of greater than 50 years for rutting. The Monte Carlo simulation gave a rutting reliability of 99.5%, meaning that there would be a 99.5% chance that the pavement would not sustain over a half inch of rutting in its 35 year design life.

The MnPAVE and MEDPG results cannot be directly compared because MEPDG predicts rutting on monthly basis (Fig. 6.2) and never reaches MnPAVE’s 0.5 inch failure criteria, while MnPAVE only predicts the life of the pavement before reaching a half inch of rutting. However, the results are consistent in that MnPAVE predicts that it will be over 50 years before a half inch of rutting occurs and MEPDG predicts less than a half inch of rutting in 600 months (50 years).

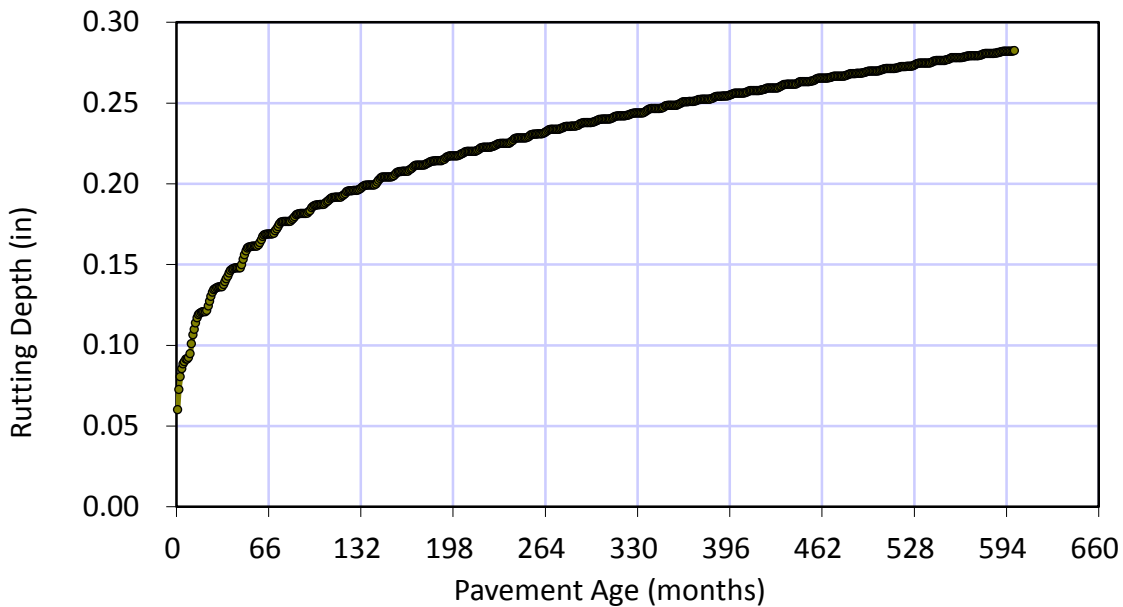


Figure 6.2: MEPDG rutting prediction for TH55-C

6.4 Modeling of TH65-C and TH65-E in MnPAVE

The TH65-C and TH65-E pavement structures were also modeled in MnPAVE. The same technique was used as was used for TH55-C. The TH65-C and TH65-E cores were taken approximately five miles apart on the same highway. Their pavement structures are identical with the exception of the SFDR layer. Their traffic information is also the same as they are covered by the same traffic report.

6.4.1 Project, Climate and Traffic Inputs

Kanabec County was selected for the project location. The MnPAVE default location for Kanabec County (45° 53' N, 93° 16' W) was used for the analysis. The climate data is shown in Table 6.3.

Table 6.3: MnPAVE climate data for TH65-C and TH65-E

	Fall	Winter	Early Spring	Late Spring	Summer
Temperature (° F)	49	20	38	59	82
Days	90	106	14	58	97

Traffic was input as 1.707 million lifetime ESALs with a 2.3% simple annual growth rate for a 35 year design period. As with the TH55-C simulation, the pavement functional type was classified as a minor arterial and MnPAVE default values were used for the axle configuration and allowable stress failure criterion sections.

6.4.2 Structure Inputs

The pavement structure was input as shown in Fig. 6.3. As with TH55-C, default values for each specific material from basic mode were used for the asphalt, aggregate base and soil layers. Dynamic modulus values for the SFDR layer were entered on advanced mode.

4" PG 58-34 Asphalt
6" SFDR
18" MnDOT Class 5 Aggregate Base
0" Sandy Loam (slightly plastic) Undisturbed Soil
Sandy Loam (slightly plastic) Undisturbed Soil

Figure 6.3: TH65-C and TH65-E pavement structure for MnPAVE

The dynamic modulus values for TH65-C and TH65-E were calculated following the procedure described in section 6.3.2. The loading time was calculated as 0.1250 seconds using Eq. 6-1. The loading frequency was calculated using Eq. 6-2 to be 12.735 Hz. The resulting dynamic modulus values for TH65-C and TH65-E are shown in Table 6.4.

Table 6.4: TH65-C and TH65-E Dynamic Modulus Values for MnPAVE

	Fall	Winter		Early Spring	Late Spring	Summer
65C E* (ksi)	437.65	470.52		452.84	420.12	362.72
65E E* (ksi)	885.57	1079.30		965.22	807.13	610.30

6.4.3 Results

MnPAVE predicted that the TH65-C pavement would have a design life of greater than 50 years before reaching one half an inch of rutting. The Monte Carlo reliability for lasting 35 years without reaching 0.5 inches of rutting is 98.2%.

MnPAVE also predicted that the TH65-E pavement would have a rutting design life of greater than 50 years. The Monte Carlo reliability for the TH65-E pavement reaching 35 years without experiencing a half an inch of rutting is 99.1%.

6.5 Comparison

A summary of the MnPAVE results for TH55-C, TH65-C and TH65-E is shown in Table 6.5. No MnPAVE simulation was performed for TH55-F because there were not enough dynamic modulus results to make a reliable master curve.

Table 6.5: MnPAVE Results

	Rutting Design Life	Rutting Reliability (35 year)
TH55-C	>50 years	99.5%
TH65-C	>50 years	98.2%
TH65-E	>50 years	99.1%

Before comparing the performances of these three pavements, it should be noted that each of these reliability analyses involved 2500 simulations. For Monte Carlo simulations, the number of simulations has a strong influence on the computed reliability. For example, if we are interested in a p -level failure probability (i.e. $1-p$ level of reliability), the coefficient of variation (CoV) that corresponds to N number of simulations is given by

$$\varepsilon\% = \sqrt{\frac{1-p}{Np}} \times 200\% \quad (6-3)$$

Consider $p = 1\%$ (or equivalently reliability level = 99%). For 2500 simulations, the CoV of the predicted failure probability is about 39%. This indicates that the simulation results could range from 99.4% to 98.61%. Therefore, the differences between the simulated reliability levels for these three pavements are slightly larger than the statistical significance of the Monte Carlo simulation. A comparison between TH65-C and TH65-E can be made because their loads and structures were identical. Table 6.5 indicates that TH65-E appears perform slightly better than TH65-C. This is consistent with the material testing results in Chapter 4 that show the TH65-E SFDR to be generally stronger than the TH65-C. Field measurements of these three sites indicated that 3-year rut depths of TH55-C, TH65-C, and TH65-E are 0.07 in, 0.09 in and 0.09 in, respectively. The relative performance of these three sites is consistent with the calculated rut reliability shown in Table 6.5.

6.6 Summary

The MnPAVE software was used to simulate the rutting performance of the SFDR project, as an alternative to the MEPDG software. The simulation of TH55-C SFDR project indicates that MnPAVE result is consistent with the MEPDG simulation. The main advantage of MnPAVE is that it allows a more flexible range of input of dynamic modulus values and at the same time it requires much less computational time compared to MEPDG. The other input parameters for MnPAVE can easily be found in MnDOT climate and traffic database. The main drawback is that MnPAVE is not able to yield the complete time-history of the rutting performance. Instead, it only gives a 35 year-reliability level for a given rutting depth (0.5 in). However, it is sufficient for the intended parametric studies, in which the reliability level could be used as an indicator of

the rutting performance instead of using the actual rutting depth. Therefore, MnPAVE can be considered as a viable option for the later parameter analysis of SFDR materials.

CHAPTER 7: PARAMETRIC ANALYSIS

A parametric analysis was conducted for the TH55-C, TH65-C and TH65-E pavement structures using MnPAVE. Dynamic modulus values ranging from one tenth to three times the experimental values were tested. Traffic values ranging from the original design traffic values up to 50 million lifetime (35-year) ESALS were also simulated. The results of the parametric analyses are shown plotted in the following sections. Tabulated results are shown in Appendix C.

7.1 Parametric analysis of TH55-C, TH65-C and TH65-E

The rutting design life results of the parametric analysis for TH55-C are plotted in Fig. 7.1. MnPAVE limits its design life prediction to 50 years, which causes the lines for the lower traffic loads to level off. Under high traffic loading, the design life appears to have an approximately linear relationship to the fraction of the experimental dynamic modulus values. It is seen that, as the ESALS reaches a value of 10 million, the rutting design life for a given E^* value exhibits a significant decrease. As expected, it is also observed that for a low ESALS value the effect of E^* on the rutting design life is more pronounced in a range of low values of E^* .

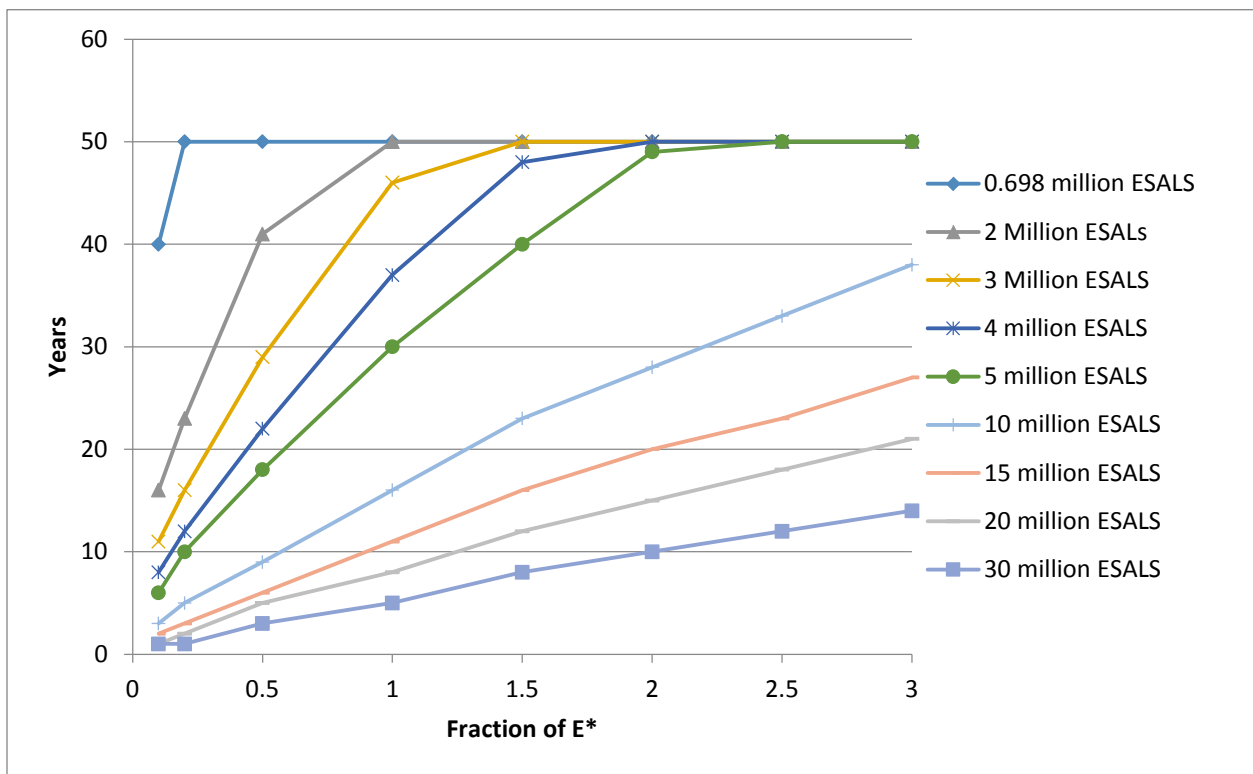


Figure 7.1: TH55-C Design Life

The rutting reliability results for TH55-C, shown in Fig. 7.2 appear similar to the design life results. Reliability increases with larger dynamic modulus values and decreases with larger amounts of traffic. Comparing Fig. 7.1 with Fig. 7.2, it is interesting to note the difference between the design life approach and reliability design approach. Consider an 0.698 million

ESAL level and a target 35 year design lifetime. If we use the design life approach (Fig. 7.1), it is seen that the design requirement can be met even with a very low value of E^* . By contrast, if we use the reliability approach, for a low value of E^* , the reliability is about 95% or equivalently 5% failure risk, which may not be acceptable. Therefore, the reliability approach offers more complete information that would allow for a performance-based design approach.

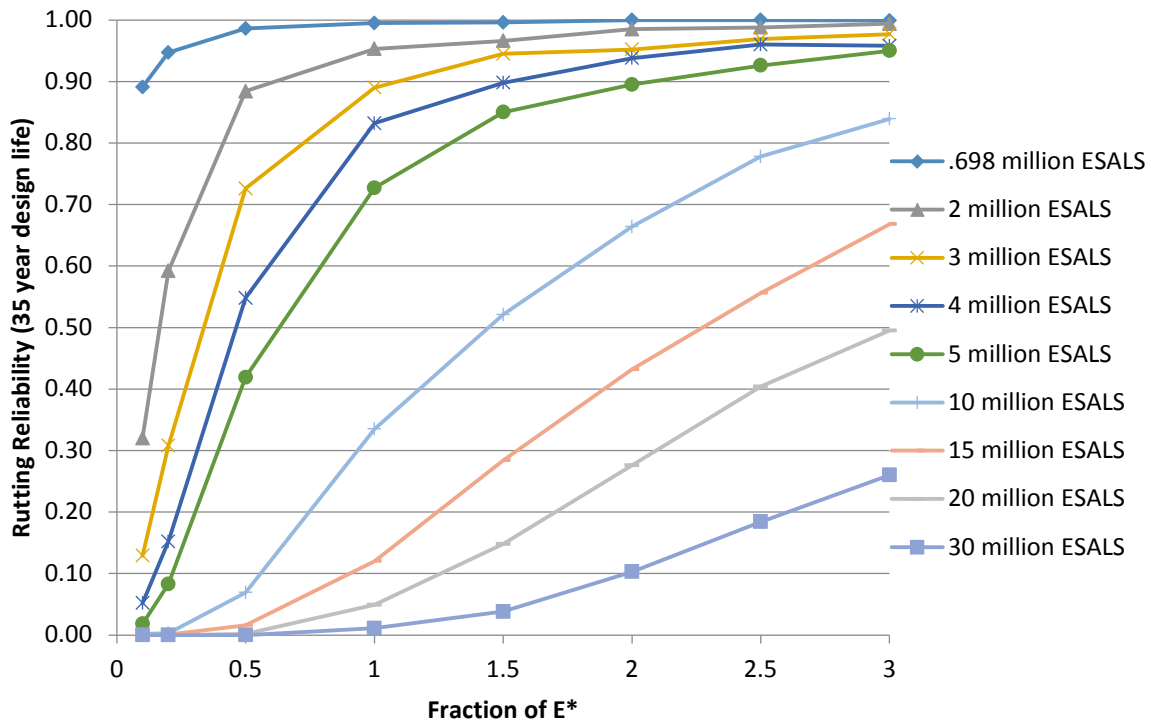


Figure 7.2: TH55-C Rutting Reliability

The rutting design life and 35 year rutting reliability results of the parametric analysis for TH65-C and TH65-E are plotted in Figs. 7.3 through 7.6. The trend of results is similar to that observed for TH55-C. It is interesting to observe again that the design life and reliability significantly decrease as the ESALS level reaches 10 million. The difference between the design life approach and the reliability design approach can also be seen in these figures.

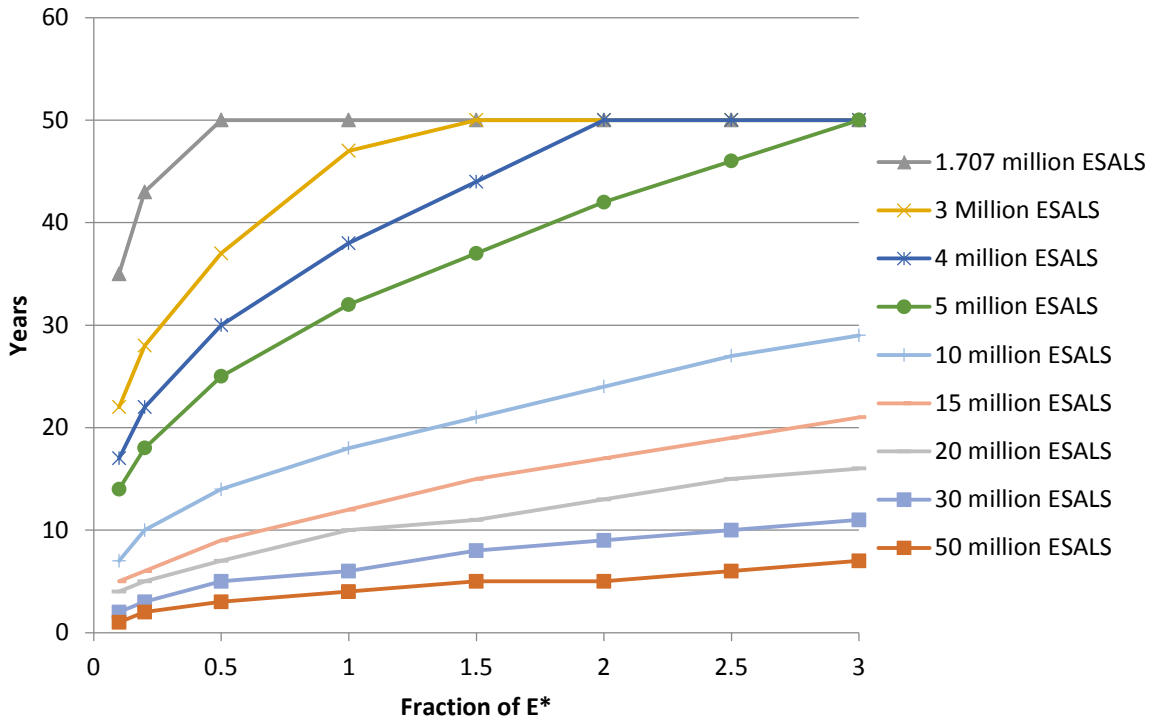


Figure 7.3: TH65-C Design Life

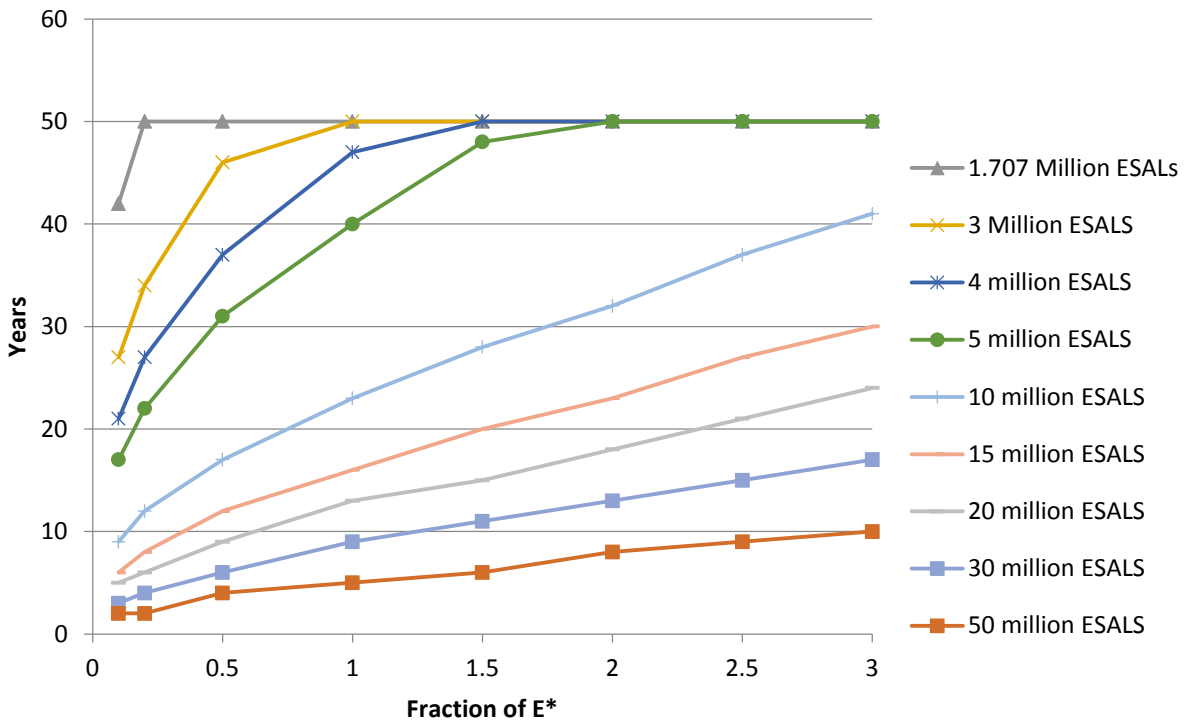


Figure 7.4: TH65-E Design Life

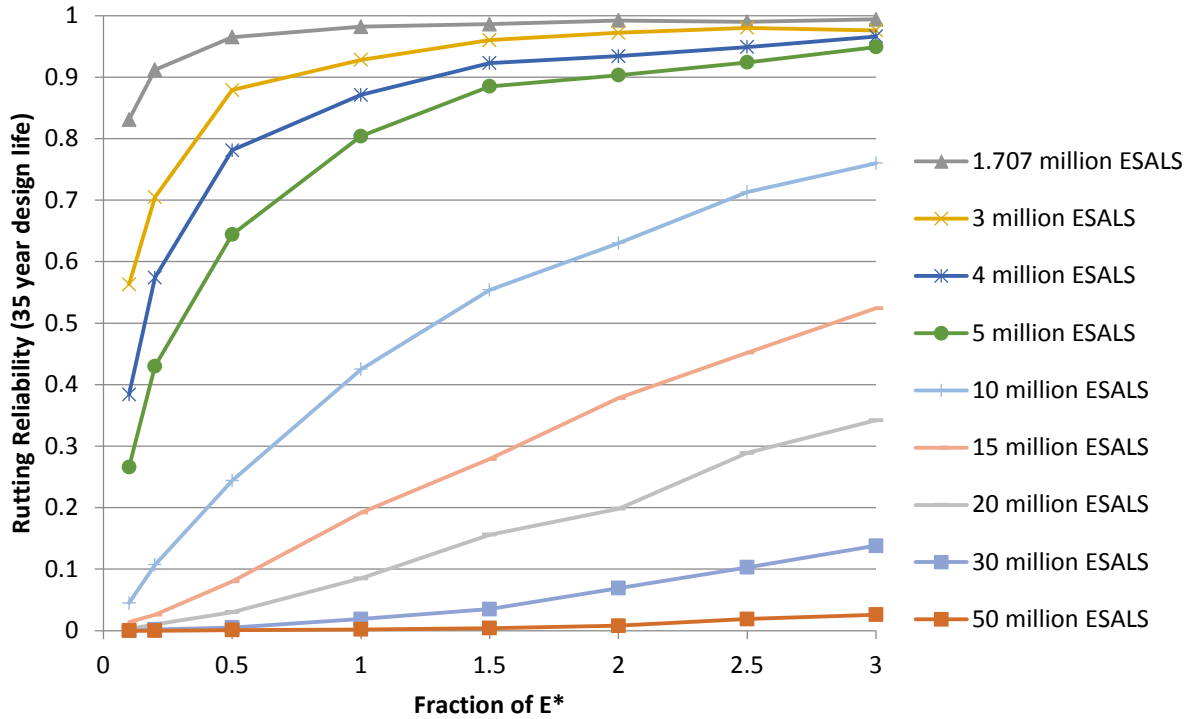


Figure 7.5: TH65-C Rutting Reliability

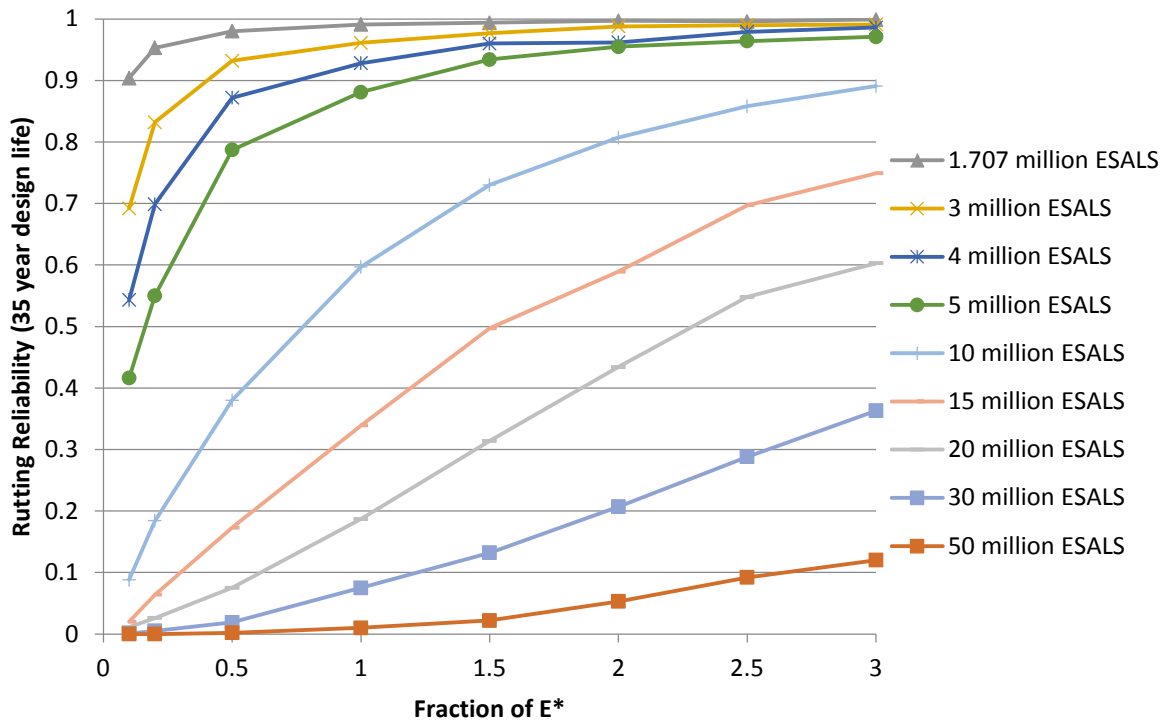


Figure 7.6: TH65-E Rutting Reliability

7.2 Comparison

The design life and reliability of the TH55-C, TH65-C, and TH65-E were plotted on the same graphs (with the original, experimental E^* values) against traffic for comparison purposes. These plots are shown in Figs. 7.7 and 7.8.

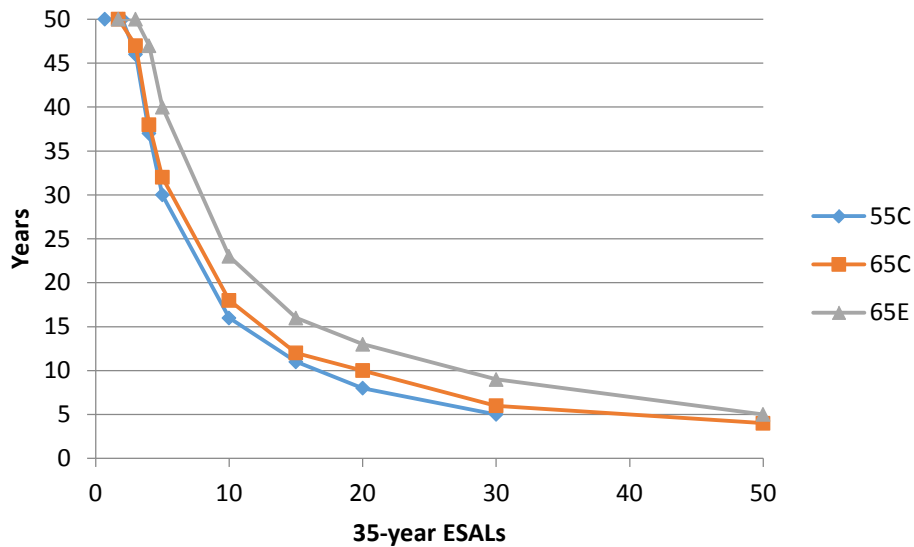


Figure 7.7: Rutting Design Life (original E^* values)

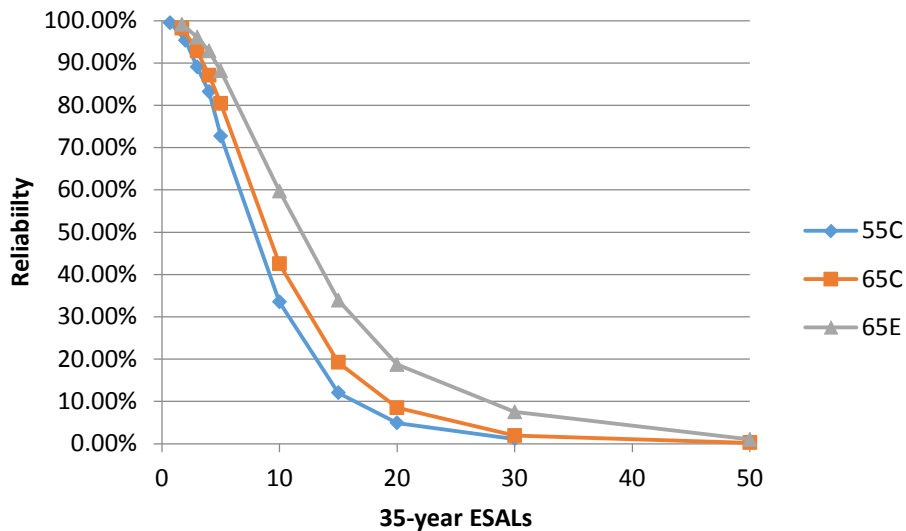


Figure 7.8: 35-Year Rutting Reliability (original E^* values)

Figs. 7.7 and 7.8 are the best way to directly compare the predicted performance of the SFDR pavement structures. TH65-C and TH65-E can be compared directly because they were modeled with the same pavement structure. Both figures clearly show that TH65-E performs better than TH65-C. Figs. 7.7 and 7.8 show that the TH65-E pavement structure performs significantly

better than the TH55-C pavement structure. It is also evident that the TH65-C pavement structure performs slightly better than the TH55C pavement structure. However, because the pavement structures are different, it is not possible to determine from the MnPAVE simulations whether the difference is caused by the SFDR formulation itself or if it is the result of a better overall pavement structure.

7.3 Summary

A series of parametric studies have been successfully performed for TH55-C, TH65-C and TH65-E, in which we considered the traffic loading and the dynamic modulus. It was shown that the design lifetime and reliability performance significantly decrease once the traffic loading is beyond a certain value. The comparison analysis indicated that the TH65-E has a better performance than TH65-C, which is consistent with the material testing results presented in Chapter 4. TH65-E also performs better than TH55-C. However, it is difficult to directly relate this comparison to the material testing results since TH65-E and TH55-C have different pavement structures. The parametric studies also revealed the implications of the application of the design life approach and the reliability-based approach on the design. It appeared that the reliability-based approach provides a complete set of information on the rutting performance of the pavement at any reliability level. This will allow engineers to determine the desirable dynamic modulus to achieve a targeted reliability level for a given pavement structure and traffic loading, which will open up opportunities for developing and implementing performance-based design approaches for SFDR.

CHAPTER 8: CONCLUSIONS

This research investigated the mechanical properties of several SFDR materials that were used in the current MnDOT projects. Meanwhile, two potential numerical tools were explored to model the SFDR structures, through which parametric studies were performed to establish the relationship between the SFDR material properties and the overall SFDR rutting performance. The findings of this research are summarized as following:

- 1) SFDR has been regarded as a cost-effective method for pavement rehabilitation. Some recommendations have been proposed on the mix design of SFDR based on the field experience. Experimental investigation of the deformation characteristics of SFDR materials has also been performed. However, there is still a lack of understanding of how the SFDR properties could influence the overall long-term behavior of the pavement, which is important for developing a method to determine the desirable SFDR properties for a given application.
- 2) The numerical studies of MnDOT cells 2, 3 and 4 indicate that SFDR materials could be best modeled as a bound asphalt layer. The simulation results compare well with measured time evolution of the rutting performance of these cells.
- 3) Several tests typically used for asphalt were performed on specimens of four different current SFDR projects, i.e. TH55-C, TH55-F, TH65-C and TH65-E. IDT creep and tension tests were performed to determine the creep compliance, Poisson's modulus and tensile strength of the SFDR. Dynamic modulus testing in the IDT position was performed to determine the dynamic modulus of the SFDR formulations. These tests were performed with varying degrees of success as the tests are designed for asphalt, not SFDR. However, the current experiments produced values for most of specimens. Overall, both the empirical behavior and the testing results showed that the TH65-E specimens were the strongest and the TH55-F specimens were the weakest.
- 4) For fracture energy test of SFDR, it was found that SCB test was unable to reach the tail portion of the load-deflection curve. Therefore, it is not possible to directly calculate the fracture energy by using the work-of-fracture method. Instead, the fracture energy was calculated by using the Irwin relationship anchored by the principle of linear elastic fracture mechanics. However, the computed values were subject to a large variation due to the scattering of both the elastic modulus and the fracture toughness. Meanwhile, the DCT tests conducted by the MnDOT Materials Office indicated that a large portion of the load-deflection could be obtained, which led to a more consistent calculation of the fracture energy.
- 5) The TH55-C pavement structure was numerically modeled by MEPDG, and the simulation result of rutting performance compared reasonably well with the field measurement. However, it was found that the MEPDG requires a specific range of dynamic modulus values, which may limit its application for SFDR. Meanwhile, MEPDG is also computationally expensive, and therefore it may not be suitable for parametric studies of SFDR performance.
- 6) Dynamic modulus testing results were also used to model the TH55-C, TH65-C and TH65-E pavement structures in MnPAVE. MnPAVE results for TH55-C were consistent

with the MEPDG results. A parametric analysis conducted in MnPAVE predicted the behavior of the TH55-C, TH65-C and TH65-E structures for a range of dynamic modulus values and traffic loadings. A comparison of the rutting results for TH55-C, TH65-C and TH65-E pavement structures with the original SFDR dynamic modulus values under a range of loads showed that TH65-E performed significantly better than TH55-C and TH65-C. This agrees with the material testing results and suggests that MnDOT could use the MnPAVE to determine the desirable properties of SFDR materials to achieve a targeted rutting performance of the pavements rehabilitated by SFDR.

REFERENCES

- [1] Bemanian, S., Polish, P., and Maurer, G. (2006). "Cold In-Place Recycling and Full-Depth Reclamation Projects by Nevada Department of Transportation: State of the Practice." *Transportation Research Record: Journal of the Transportation Research Board*, 1949: 54 – 71.
- [2] Mallick, R. B., Bonner, D. S., Bradbury, R. L., Andrews, J. O., Kandhal, P. S., and Kearney, E. J. (2002). "Evaluation of Performance of Full-Depth Reclamation Mixes." *Transportation Research Record: Journal of the Transportation Research Board*, 1809: 199 – 208.
- [3] Lewis, D. E., Jared, D. M., Torres, H., and Mathews, M. (2006). "Georgia's Use of Cement-Stabilized Reclaimed Base in Full-Depth Reclamation." *Transportation Research Record: Journal of the Transportation Research Board*, 1952: 125 – 133.
- [4] "Cement-Treated, Full-Depth Reclamation Method Extends Pavement Life." (2008). *Concrete Products*, 111(2), 15.
- [5] "Everything in Green." (2011). *Roads & Bridges*, 49(9), 48 – 51.
- [6] Landers, K. (2001). "Rebuilding by Reclaiming: The FDR Process." *Better Roads Magazine*, 72(7): 6 – 9.
- [7] Kearney, E. J., and Huffman, J. E. (1999). "Full-Depth Reclamation Process." *Transportation Research Record: Journal of the Transportation Research Board*, 1684: 203 – 209.
- [8] Lewis, D. (2004). "Recycling whole roads!" Presented at Georgia Quality Initiative Workshop.
- [9] Epps, J. A. (1990). "NCHRP Synthesis of Highway Practice 160: Cold-Recycled Bituminous Concrete Using Bituminous Materials." *NCHRP Synthesis of Highway Practice*, 1990-7: 111.
- [10] Scullion, T., Sebesta, S., Estakhri, C., Harris, P., Shon, C., Harvey, O., et al. (2012). "Full-Depth Reclamation: New Test Procedures and Recommended Updates to Specifications." Texas Transportation Institute, College Station, TX.
- [11] *Basic asphalt recycling manual*. (2001). Asphalt Recycling and Reclaiming Association, Annapolis, MD.
- [12] 2013. Investigation of Optimal Mix Design of Full Depth Reclamation Stabilization with Cement and Emulsion: Project Proposal Form. Minnesota Department of Transportation – Minnesota Local Road Research Board. St. Paul, MN.
- [13] Mallick, R. B., Teto, M. R., Kandhal, P. S., Brown, E. R., Bradbury, R. L., and Kearney, E. J. (2002). "Laboratory Study of Full-Depth Reclamation Mixes." *Transportation Research Record*, (1813), 103 – 110.
- [14] Ryan, N. (2010). "Y=FDR." *Roads and Bridges*, 48(2): 30-32.
- [15] Reclaiming the streets. (2007). *Roads and Bridges*, 45(10), 46.
- [16] Dixon, P., Guthrie, W., and Eggett, D. (2012). "Factors Affecting Strength of Road Base Stabilized with cement Slurry or Dry Cement in Conjunction with Full-Depth Reclamation." *Transportation Research Record*, No. 2310: 113- 120.
- [17] Diefenderfer, B. K., and Apeageyi, A. K. (2011). "Analysis of Full-Depth Reclamation Trial Sections in Virginia". Virginia Center for Transportation: Innovation and Research, Charlottesville, VA.
- [18] "Full-depth report: Washington state uses cement for failed pavements." (2006). *Roads and Bridges*. 76.
- [19] Harris, S. (2007). "Reusing Roadways." *Roads and Bridges*. 45(5): 60-63.
- [20] "Lebanon, Ohio uses FDR to Quell Reflective Cracks." (2012). *Pavement Preservation Journal*. 5(6): 37 – 39.

- [21] Shatnawi, S. (2012). "Implementing In-Place Recycling Technologies". *Pavement Preservation Journal*, 5(5): 33-35.
- [22] Smith, C. R., Lewis, D. E., Turner, J., and Jared, D. M. (2008). "Georgia's Use of Lime in Full-Depth Reclamation." *Transportation Research Record*, 2059:89 – 94.
- [23] 2012. *Lime and soil stabilization*. Internet. Accessed date: 09/23/2013, URL: http://www.lime.org/uses_of_lime/construction/soil.asp
- [24] Thompson, M. R. (1970)." Suggested Method of Mixture Design Procedure for Lime Treated Soils." ASTM, Special Technical Publication 479. ASTM International, West Conshohocken, PA.
- [25] Attia, M., Abdelrahman, M., and Alam, T. (2009). "Investigation of Stripping in Minnesota Class 7 (RAP) and Full-Depth Reclamation Base Materials". Minnesota Department of Transportation, St. Paul, MN.
- [26] Kim, W. and Labuz, J. F. (2007). Resilient Modulus and Strength of Base Course with Recycled Bituminous Material, Report No. MN/RC-2007-05, Minnesota Department of Transportation, St. Paul, MN.
- [27] 2005. "Guidelines for Asphalt Emulsion Full Depth Reclamation (FDR) and Granular Base Stabilization (GBS)." Road Science, Tulsa, OK.
- [28] Dunlap, W. A. (1963). A Report on a Mathematical Model Describing the Deformation Characteristics of Granular Materials. Texas Transp. Inst., Tech. Rep. No. 1, Proj. 2-8-62-26, Texas A&M University, College Station, TX.
- [29] Monismith, C. L., Seed, H. B., Mitry, F. G., and Chan, C. K.. Prediction of Pavement Deflections from Laboratory Tests. *Second International Conference on the Structural Design of Asphalt Pavements*, Ann Arbor, MI, 1967: 53 – 88.
- [30] Hicks, R.G. (1970). Factors Influencing the Resilient Properties of Granular Materials. Ph.D. thesis, University of California, Berkeley, CA.
- [31] Seed, H. B., Mitry, F. G., Monismith, C. L., and Chan, C. K. (1967). Prediction of Flexible Pavement Deflections from Laboratory Repeated Load Tests. NCHRP Rep. No. 35, National Cooperative Highway Research Program.
- [32] Uzan, J. (1985). "Characterization of Granular Material." *Transportation Research Record*. 1022: 52 – 59.
- [33] Velasquez, R., Hoegh, K., Yut, I., Funk, N., Cochran, G., Marasteanu, M., and Khazanovich, L. Implementation of the MEPDG for New and Rehabilitated Pavement Structures for Design of Concrete and Asphalt Pavements in Minnesota. (2009). Report No. MN/RC 2009-06. Minnesota Department of Transportation, St. Paul, MN.
- [34] United States Geological Survey (2014). *Water Resources of the United States*. Internet. Accessed date: 01/30/2015. URL: <http://www.usgs.gov/water/>
- [35] Standard Method of Test for Determining the Creep Compliance and Strength of Hot-Mix Asphalt (HMA) Using the Indirect Tension Test Device: T322-03. 2006. AASHTO, Washington, DC.
- [36] Standard Method of Test for Determining Dynamic Modulus of Hot-Mix Asphalt Concrete Mixtures: TP 62-03. 2006. AASHTO, Washington, DC.
- [37] Kim, Y., Seo, Y., King, M., and Momen, M. (2004). "Dynamic Modulus Testing of Asphalt Concrete in Indirect Tension Mode," *Transportation Research Record*, 1981: 163 – 173.
- [38] ARA, Inc. (2004). *Guide for Mechanistic-Empirical Design of New and Rehabilitated Pavement Structures: NCHRP 1-37A*. National Cooperative Highway Research Program, Transportation Research Board National Research Council, Washington, DC.

- [39] Rowe, G. M., Khoei, S. H., Blankenship, P. and Mahboub, K. C. (2009). "Evaluation of Aspects of E* Test by Using Hot-Mix Asphalt Specimens with Varying Void Contents." *Transportation Research Record*, 2127: 164 – 172.
- [40] *Standard Method of Test for Determining the Fracture Energy of Asphalt Mixtures Using the Semi Circular Bend Geometry (SCB)*. AASHTO, Washington, DC.
- [41] Marasteanu, M. O., Zofka, A., Turos, M., Li, X., Velasquez, R., Buttlar, W., Paulino, G., Braham, A., Dave, E., Ojo, J., Bahia, H., Bausano, C. J., Gallistel, A., and McGraw, J. (2007) Investigation of Low Temperature Cracking in Asphalt Pavements: National Pooled Fund Study 776. Final Report. Minnesota Department of Transportation, St. Paul, MN.
- [42] Le, J.-L., Cannone Falchetto, A., and Marasteanu, M. O. (2013) "Determination of Strength Distribution of Quasibrittle Structures from Size Effect Analysis", *Mechanics of Materials*, 66: 79 – 87.
- [43] Lim, I. L., Johnson, I. W. and Choi, S. K. (1993) "Stress Intensity Factor for Semi-Circular Specimen Under Three-Point Bending", *Engineering Fracture Mechanics*, 44(3), 363 – 382.
- [44] Li, X. and Marasteanu, M. O. (2004) "Evaluation of Low Temperature Fracture Resistance of Asphalt Mixtures Using the Semi-Circular Bend Test," *Journal of the Association of Asphalt Paving Technologists*, 73, 401-426.
- [45] Minnesota Department of Transportation. "Speed Limits in Minnesota." Internet. Accessed date: 4/1/ 2015. URL: <http://www.dot.state.mn.us/speed/>.
- [46] Das, B. M. (2000). *Fundamentals of Geotechnical Engineering*. 2nd ed. Toronto, Ontario: Nelson/Thompson.
- [47] Minnesota Department of Transportation (2007) *Pavement Manual* Internet. URL: http://www.dot.state.mn.us/materials/pvmtdesign/docs/2007manual/Chapter_3-2.pdf
- [48] Valasquez, R., Hoegh, K., Yut, I. Funk, N., Cochran, G., Marasteanu, M., and Khazanovich, L. (2009). Implementation of the MEPDG for New and Rehabilitated Pavement Structures for Design of Concrete and Asphalt Pavements in Minnesota. Final Report. Minnesota Department of Transportation, St. Paul, MN.
- [49] Brown, S. F. (1973), "Determination of Young's Modulus for Bituminous Materials in Pavement Design," *Highway Research Record 431*: 38 – 49.
- [50] Al-Qadi, I. L., Xie, W., and Mostafa, M. A. (2008), "Frequency Determination from Vehicular Loading Time Pulse to Predict Appropriate Complex Modulus in MEPDG", *Journal of the Association of Asphalt Paving Technologists* 77, 739 – 772.
- [51] Garcia, G.S. (2007), Concepts for Mechanistic-Empirical Design Procedure for Extended Hot Mix Asphalt Pavements with a Multi-Layered Structure. Ph.D. Dissertation, University of Illinois at Urbana-Champaign, Urbana, Illinois.

**APPENDIX A:
MEPDG Inputs**

This appendix contains material parameters values used for modeling MnROAD cells 2, 3, and 4 in the MEPDG. The values of $|E^*|$ for the asphalt mixture and $|G^*|$ for the PG 64-34 asphalt binder used in this analysis are shown in Tables A.1 and A.2.

Table A.1: Complex modulus $|E^*|$ values (psi) for asphalt concrete

T(F) / Frequency (Hz)	0.1	0.5	1	5	10	25
14	1701632	2161074	2367529	2868209	3090528	3287345
40	397123	614729	737445	1098021	1277741	1533229
70	79450	131132	167171	313858	401981	552609
100	29955	40026	47735	82948	117681	195277
130	22494	26408	28964	38991	51821	88026

Table A.2: Complex shear modulus $|G^*|$ and phase angle at 10rad/s for PG 64-34 asphalt binder

T(F)	G^* (Pa)	Phase Angle (°)
93.2	83500	61.01
104	39100	61.24
114.8	19710	61.2
125.6	10620	61.42
136.4	5926	62.19
147.2	3414	63.58
158	1986	65.47

Each of the three cells was stabilized using the same engineered emulsion. The values of $|G^*|$ used for the SFDR layer in the three cells are reported in Table 9.

Table A.3: Binder complex shear modulus $|G^*|$ at 10rad/s for the engineered emulsion stabilizer in the SFDR layer

T(F)	G^* (Pa)	Phase Angle (°)
104	4473	84.4
114.8	2398	85.8
125.6	1073	87.3

The $|E^*|$ values used when SFDR was modeled as a bound asphalt layer are summarized in tables A.4, A.5 and A.6.

Table A.4: Complex modulus $|E^*|$ values (psi) for the SFDR layer of cell 2

T (F)/ Frequency (Hz)	0.1	0.5	1	5	10	25
14	715537	823052	867842	972942	1011406	1065520
40	360824	460911	506155	642428	699943	747723
70	97066	146535	177279	272587	317041	371615
100	46529	63996	75602	123117	147868	192847
130	26527	32943	37069	54148	65300	91920

Table A.5: Complex modulus $|E^*|$ values (psi) for the SFDR layer of cell 3

T (F)/Frequency (Hz)	0.1	0.5	1	5	10	25
14	1338553	1491181	1558990	1725834	1740648	1747731
40	814011	1002423	1089893	1324776	1409468	1562775
70	197369	294434	347984	513123	586599	678118
100	66056	101639	127195	216162	269280	354113
130	36203	46178	54357	83319	102182	139425

Table A.6: Complex modulus $|E^*|$ values (psi) for the SFDR layer of cell 4

T (F)/ Frequency (Hz)	0.1	0.5	1	5	10	25
14	1193162	1402779	1465428	1680946	1742618	1891526
40	514782	650460	716483	931747	1020409	1098273
70	163312	244149	288824	430812	502265	574846
100	58101	87144	107176	176226	218173	282609
130	27619	35542	42086	65863	85766	129068

The results of the sensitivity analysis for the binder complex shear modulus $|G^*|$ are reported in Figure 5. $|G^*|$ was varied from $0.1 \cdot (G^*_{lab})$ to $500 \cdot (G^*_{lab})$ where G^*_{lab} represents the lab value of $|G^*|$ reported by MnDOT. Each data point in the figure represents a separate run in the MEPDG using a different $|G^*|$ value. The total rutting 20 years after construction is reported.

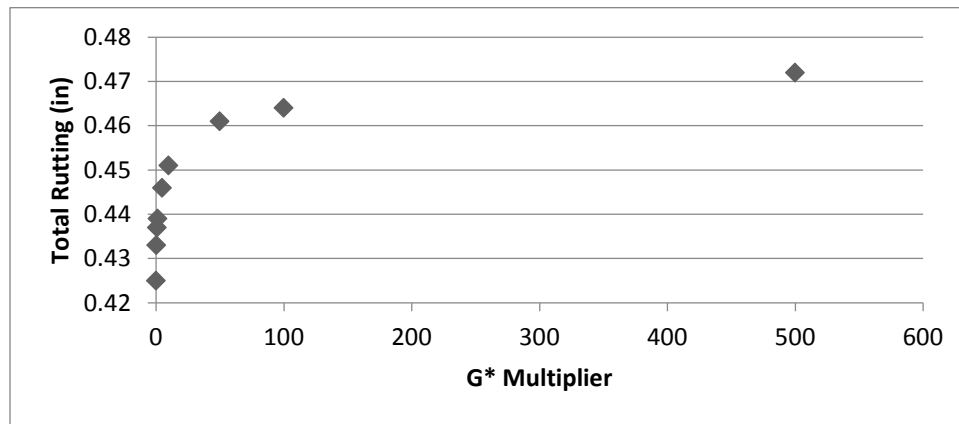


Figure A.1: Sensitivity analysis of the binder complex shear modulus $|G^*|$

APPENDIX B:
Individual Specimen Testing Results

This appendix contains material testing results for the individual specimens.

IDT Test Results

Table B.1: Creep Compliance (GPa⁻¹) – TH 55

Time of Loading (s)	55-CF	55-CT	55-FB	55-FF	55-FP
1	0.3931	0.3245	0.5099	0.3074	0.6079
2	0.4252	0.3500	0.5591	0.4817	0.6947
5	0.4310	0.3839	0.6239	0.5611	0.7903
10	0.4397	0.4030	0.6575	0.6328	0.8540
20	0.4601	0.3945	0.7111	0.6713	0.9437
50	0.4747	0.4348	0.8587	0.7814	1.1203
100	0.5854	0.4454	0.9348	0.8557	1.2766

Table B.2: Creep Compliance (GPa⁻¹) – TH 65

Time of Loading (s)	65-CD	65-CE	65-CQ	65-EJ	65-EM	65-ES
1	0.274	1.518	0.175	0.1104	0.0606	0.0951
2	0.292	2.089	0.204	0.1681	0.0839	0.1146
5	0.313	2.397	0.215	0.1844	0.0963	0.1180
10	0.354	2.674	0.217	0.1920	0.1001	0.1238
20	0.388	3.043	0.226	0.2083	0.1006	0.1329
50	0.401	3.765	0.245	0.2095	0.1093	0.1387
100	0.460	4.566	0.267	0.1957	0.1120	0.1283

Note: The creep compliance and Poisson’s ratio for 65-CE were calculated but were excluded from the averages because of extremely high values. It is believed that the LVDT disconnected from the specimen during the test.

Table B.3: Poisson’s Ratio – TH 55

Time of Loading (s)	55-CF	55-CT	55-FB	55-FF	55-FP
1	0.251	0.501	0.241	0.534	0.097
2	0.258	0.543	0.230	0.591	0.096
5	0.218	0.614	0.259	0.663	0.117
10	0.203	0.656	0.256	0.791	0.126
20	0.201	0.520	0.263	0.719	0.147
50	0.177	0.592	0.369	0.784	0.196
100	0.323	0.548	0.361	0.741	0.238

Table B.4: Poisson's Ratio – TH 65

Time of Loading (s)	65-CD	65-CE	65-CQ	65-EJ	65-EM	65-ES
1	0.081	4.675	0.430	0.081	0.320	0.231
2	0.063	5.980	0.439	0.112	0.285	0.203
5	0.065	7.040	0.426	0.140	0.378	0.228
10	0.099	7.973	0.385	0.134	0.397	0.244
20	0.128	9.196	0.378	0.171	0.343	0.293
50	0.117	11.422	0.404	0.140	0.389	0.284
100	0.191	13.719	0.464	0.078	0.369	0.168

Table B.5: Tensile Strength

Specimen	Tensile Strength (MPa)
55-CE	0.331
55-CF	0.257
55-CT	0.373
55-FB	0.202
55-FF	0.187
55-FP	0.197
65-CD	0.416
65-CE	0.267
65-CQ	0.382
65-EJ	0.991
65-EM	0.938
65-ES	0.955

Dynamic Modulus Individual Specimen Results

The original values of a dynamic modulus for each specimen at each frequency and temperature are shown in Tables B.6 through B.8. Some values are missing because the tests were not able to be completed at the highest temperatures and frequencies.

Table B.6: Dynamic modulus values (GPa) at -10°C

Freq.	25	10	5	1	0.5	0.1	0.05	0.01
65-EC	6.9898	8.1800	8.0133	7.9776	7.7592	7.5829	7.0213	7.0293
65-EH	7.7903	7.6585	7.5076	5.8026	7.2192	6.8918	6.5301	6.5012
65-ET	7.4979	8.6159	8.1959	7.4792	7.2805	6.8665	6.1939	5.7059
55-CL	2.7459	3.3332	3.3816	2.6898	2.6158	2.9115	2.6824	2.4911
55-CR	3.4143	3.8148	3.9302	4.1861	3.9879	3.9771	3.8299	3.6225
55-CD	2.3974	2.4565	2.3437	2.1838	2.1071	2.0021	2.0184	1.8951
55-FE	3.7346	4.1921	4.1912	3.8588	3.6590	3.2547	3.1704	2.8689
55-FC	2.0483	2.0805	1.9977	1.7306	1.6681	1.5320	1.4952	1.3548
65-CT	3.9308	4.7446	4.6712	4.1797	4.0485	3.8928	3.8680	3.7373
65-CN	3.3744	4.1068	3.8920	3.2837	3.0238	3.4885	3.3101	3.3321
65-CO	2.4578	2.3288	2.2629	2.0749	2.0449	1.9321	1.8664	1.8080

Table B.7: Dynamic modulus values (GPa) at +10°C

Freq.	25	10	5	1	0.5	0.1	0.05	0.01
65-EC	4.3763	5.8578	5.5786	5.3909	5.1243	4.6604	4.4957	4.2290
65-EH	5.7321	5.7343	5.6237	5.0310	4.8020	4.4907	4.1416	3.8009
65-ET	5.9212	6.4015	5.9976	5.1437	4.7540	4.1975	3.9491	3.6283
55-CL	1.9472	2.8991	2.7526	2.1920	2.1110	1.9324	1.8047	1.7368
55-CR	3.5268	3.6649	3.5030	3.2481	3.0035	2.9271	2.7605	2.6189
55-CD	1.2065	3.0845	3.0096	2.5458	2.4399	2.2567	2.1839	1.9727
55-FE	2.4687	2.3896	2.2928	1.9924	1.8477	1.5715	1.4566	1.2764
55-FC	1.3814	1.4273	1.5569	1.6958	1.9827	7.6609	-2.1622	
65-CT	2.7989	3.9382	3.7309	3.0750	3.2178	3.0693	2.9177	2.6419
65-CN	2.1002	2.0666	2.0398	2.0373	2.0155	1.8164	1.8198	1.5968
65-CO	2.5990	2.8870	2.6759	2.3730	2.1820	2.0112	1.8591	1.6342

Table B.8: Dynamic modulus values (GPa) at +35°C

Freq.	25	10	5	1	0.5	0.1	0.05	0.01
65-EC	3.6445	3.6747	3.4875	2.8529	2.7882	2.3742	2.1794	1.9308
65-EH	3.9819	3.4674	3.3978	3.1346	2.7626	2.3798	2.1715	1.8641
65-ET	3.8187	3.5071	3.3788	2.4880	2.3033	2.0231	1.9223	1.6757
55-CL	1.9404	1.9476	1.8049	1.5808	1.4297	1.3187	1.2122	1.0729
55-CR	2.4567	1.4192	2.6163	2.2277	2.1350	1.8346	1.7728	1.5588
55-CD	1.3284	1.3637	1.3176	1.0534	0.9647	0.8507	0.7770	0.6804
55-FE	1.6669	-0.8144	1.6137	2.0424	2.5463			
55-FC								
65-CT	2.4907	2.4156	2.3215	1.8478	1.7051	1.5107	1.3910	1.1668
65-CN	1.7699	1.5689	1.5437	1.3543	1.2243	0.9803	0.9597	0.9267
65-CO	0.8694	3.5993	4.0522	3.4988	2.9047	1.3275	1.2236	0.9715

Table B.9: Full DCT Results

Highway	Sample Set ID	Sample ID	Date	Test Length	Fracture Energy	Max Load
TH65	2014-005-02-01 "CSS-1 w/ Cement"	2014-005-02-01-CR-SFDR1	3/9/2015	23.16	14.58	0.237
TH65	2014-005-02-02 "EE w/ Cement"	2014-005-02-02-EA-SFDR1	3/9/2015	48.36	46.63	0.441
TH65	2014-005-02-02 "EE w/ Cement"	2014-005-02-02-EA-SFDR2	3/9/2015	47.64	59.35	0.639
TH65	2014-005-02-02 "EE w/ Cement"	2014-005-02-02-EE-SFDR1	3/10/2015	52.64	62.29	0.742
TH65	2014-005-02-02 "EE w/ Cement"	2014-005-02-02-EE-SFDR2	3/10/2015	48.84	55.7	0.729
TH65	2014-005-02-02 "EE w/ Cement"	2014-005-02-02-EP-SFDR1	3/10/2015	73.26	86.7	0.558
TH65	2014-005-02-02 "EE w/ Cement"	2014-005-02-02-EP-SFDR2	3/10/2015	59.4	60.45	0.607
TH65	2014-005-02-02 "EE w/ Cement"	2014-005-02-02-EQ-SFDR2	3/17/2015	32.84	30.32	0.394
TH56 (S of Kenyon)	2014-005-04 Crack-B "EE"	2014-005-04-CB1-SFDR1	1/23/2015	89.68	188.49	2.156
TH56 (S of Kenyon)	2014-005-04 Crack-B "EE"	2014-005-04-CB1-SFDR2	1/23/2015	100.08	177.93	1.365
TH56 (S of Kenyon)	2014-005-04 Crack-B "EE"	2014-005-04-CB2-SFDR1	1/23/2015	107.68	256.7	1.954
TH56 (S of Kenyon)	2014-005-04 Crack-B "EE"	2014-005-04-CB2-SFDR2	1/23/2015	70.04	164.08	1.746
TH56 (S of Kenyon)	2014-005-04 Crack-B "EE"	2014-005-04-CB3-SFDR1	1/23/2015	78.08	190.89	2.1
TH56 (S of Kenyon)	2014-005-04 Crack-B "EE"	2014-005-04-CB4-SFDR1	1/23/2015	78.4	177.48	2.342
TH56 (S of Kenyon)	2014-005-04 Crack-B "EE"	2014-005-04-CB4-SFDR2	1/23/2015	76.28	165.4	1.555
TH56 (S of Kenyon)	2014-005-04 Crack-C "EE"	2014-005-04-CC2-SFDR1	3/17/2015	86.96	208.62	2.102
TH56 (S of Kenyon)	2014-005-04 Crack-C "EE"	2014-005-04-CC2-SFDR2	3/17/2015	134.36	198.92	1.531
TH56 (S of Kenyon)	2014-005-04 Crack-D "EE"	2014-005-04-CD1-SFDR1	1/27/2015	63	146.87	2.268
TH56 (S of Kenyon)	2014-005-04 Crack-D "EE"	2014-005-04-CD1-SFDR2	1/27/2015	94.76	180.12	1.39
TH56 (S of Kenyon)	2014-005-04 Crack-D "EE"	2014-005-04-CD2-SFDR1	1/27/2015	73.64	173.62	1.646
TH56 (S of Kenyon)	2014-005-04 Crack-D "EE"	2014-005-04-CD3-SFDR1	1/27/2015	96.08	229.83	2.13
TH56 (S of Kenyon)	2014-005-04 Crack-D "EE"	2014-005-04-CD3-SFDR2	1/29/2015	95.64	197.35	1.553
TH56 (S of Kenyon)	2014-005-04 Crack-D "EE"	2014-005-04-CD4-SFDR1	1/29/2015	125.68	233.28	1.564
TH56 (S of Kenyon)	2014-005-04 Crack-D "EE"	2014-005-04-CD4-SFDR2	1/29/2015	93.12	169.5	1.218
TH56 (S of Kenyon)	2014-005-04 Good Pvmt-G "EE"	2014-005-04-G3-SFDR1	3/17/2015	95.68	222.12	1.766
TH56 (S of Kenyon)	2014-005-04 Good Pvmt-G "EE"	2014-005-04-G3-SFDR2	3/17/2015	108.44	157.87	1.013
TH56 (S of Kenyon)	2014-005-04 Good Pvmt-G "EE"	2014-005-04-G6-SFDR2	3/17/2015	69.88	117.89	1.304
TH56 (S of Kenyon)	2014-005-04 Good Pvmt-G "EE"	2014-005-04-G11-SFDR1	3/17/2015	102.36	193.71	1.895
TH56 (S of Kenyon)	2014-005-04 Good Pvmt-G "EE"	2014-005-04-G11-SFDR2	3/17/2015	88.92	175.66	1.411
TH56 (N of Kenyon)	014-005-05-01 Northbound Lane "EE"	2014-005-05-01-B-SFDDR1	3/16/2015	103.56	168.97	1.279
TH56 (N of Kenyon)	014-005-05-01 Northbound Lane "EE"	2014-005-05-01-B-SFDDR2	3/16/2015	81.36	189.21	2.256
TH56 (N of Kenyon)	014-005-05-01 Northbound Lane "EE"	2014-005-05-01-F-SFDDR1	3/16/2015	75.32	180.34	2.372
TH56 (N of Kenyon)	014-005-05-01 Northbound Lane "EE"	2014-005-05-01-F-SFDDR2	3/16/2015	63.4	121.88	1.583
TH56 (N of Kenyon)	014-005-05-02 Southbound Lane "EE"	2014-005-05-02-J-SFDR1	3/16/2015	74.4	130.03	1.357
TH56 (N of Kenyon)	014-005-05-02 Southbound Lane "EE"	2014-005-05-02-J-SFDR2	3/16/2015	105.24	258.19	1.475
TH56 (N of Kenyon)	014-005-05-02 Southbound Lane "EE"	2014-005-05-02-Q-SFDR1	3/16/2015	94.56	170.42	1.275
TH56 (N of Kenyon)	014-005-05-02 Southbound Lane "EE"	2014-005-05-02-Q-SFDR2	3/16/2015	86.8	134.13	1.133

APPENDIX C:
Full MnPAVE Results

This appendix contains the full results of the parametric analysis performed using MnPAVE.

Table C.1: TH55-C Design Life (years)

Million ESALs\E* multiplier	0.1	0.2	0.5	1	1.5	2	2.5	3
0.698	40	50	50	50	50	50	50	50
2	16	23	41	50	50	50	50	50
3	11	16	29	46	50	50	50	50
4	8	12	22	37	48	50	50	50
5	6	10	18	30	40	49	50	50
10	3	5	9	16	23	28	33	38
15	2	3	6	11	16	20	23	27
20	1	2	5	8	12	15	18	21
30	1	1	3	5	8	10	12	14

Table C.2: TH55-C Rutting Reliability

Million ESALs\E* multiplier	0.1	0.2	0.5	1	1.5	2	2.5	3
0.698	89.10%	94.70%	98.60%	99.50%	99.60%	100.00%	100.00%	99.90%
2	32.00%	59.20%	88.40%	95.30%	96.60%	98.50%	98.80%	99.40%
3	12.90%	30.80%	72.60%	89.00%	94.50%	95.20%	96.90%	97.70%
4	5.20%	15.20%	54.80%	83.20%	89.80%	93.80%	96.00%	95.80%
5	1.80%	8.30%	41.90%	72.70%	85.00%	89.50%	92.60%	95.00%
10	0.20%	0.30%	6.90%	33.50%	52.10%	66.40%	77.80%	83.90%
15	0.00%	0.10%	1.60%	12.00%	28.40%	43.20%	55.60%	66.80%
20	0.00%	0.00%	0.20%	4.90%	14.80%	27.60%	40.40%	49.50%
30	0.00%	0.00%	0.00%	1.10%	3.80%	10.30%	18.40%	26.00%

Table C.3: TH65-C Design Life (years)

Million ESALs\E* multiplier	0.1	0.2	0.5	1	1.5	2	2.5	3
1.707	35	43	50	50	50	50	50	50
3	22	28	37	47	50	50	50	50
4	17	22	30	38	44	50	50	50
5	14	18	25	32	37	42	46	50
10	7	10	14	18	21	24	27	29
15	5	6	9	12	15	17	19	21
20	4	5	7	10	11	13	15	16
30	2	3	5	6	8	9	10	11
50	1	2	3	4	5	5	6	7

Table C.4: TH65-C Rutting Reliability

Million ESALs\E* multiplier	0.1	0.2	0.5	1	1.5	2	2.5	3
1.717	83.10%	91.20%	96.50%	98.20%	98.60%	99.20%	99.00%	99.40%
3	56.30%	70.50%	87.90%	92.80%	96.00%	97.20%	98.00%	97.60%
4	38.40%	57.40%	78.10%	87.10%	92.30%	93.40%	94.90%	96.60%
5	26.60%	43.00%	64.40%	80.40%	88.50%	90.30%	92.40%	94.90%
10	4.50%	10.70%	24.40%	42.50%	55.40%	63.00%	71.30%	76.00%
15	1.40%	2.60%	8.00%	19.20%	27.90%	37.80%	45.20%	52.40%
20	0.30%	1.00%	3.00%	8.50%	15.60%	19.80%	28.90%	34.20%
30	0.00%	0.20%	0.50%	1.90%	3.50%	6.90%	10.30%	13.80%
50	0.00%	0.00%	0.10%	0.20%	0.40%	0.80%	1.90%	2.60%

Table C.5: TH65-E Design Life (years)

Million ESALs\E* multiplier	0.1	0.2	0.5	1	1.5	2	2.5	3
1.707	42	50	50	50	50	50	50	50
3	27	34	46	50	50	50	50	50
4	21	27	37	47	50	50	50	50
5	17	22	31	40	48	50	50	50
10	9	12	17	23	28	32	37	41
15	6	8	12	16	20	23	27	30
20	5	6	9	13	15	18	21	24
30	3	4	6	9	11	13	15	17
50	2	2	4	5	6	8	9	10

Table C.6: TH65-E Rutting Reliability

Million ESALs\E* multiplier	0.1	0.2	0.5	1	1.5	2	2.5	3
1.717	90.40%	95.30%	98.00%	99.10%	99.40%	99.70%	99.60%	99.90%
3	69.20%	83.20%	93.20%	96.10%	97.70%	98.80%	99.00%	99.10%
4	54.30%	69.90%	87.20%	92.80%	96.00%	96.20%	97.90%	98.60%
5	41.60%	55.00%	78.70%	88.10%	93.40%	95.50%	96.40%	97.10%
10	8.80%	18.40%	38.00%	59.70%	73.00%	80.70%	85.80%	89.10%
15	2.00%	6.40%	17.30%	33.90%	49.70%	58.90%	69.70%	74.90%
20	1.10%	2.60%	7.50%	18.70%	31.40%	43.40%	54.80%	60.30%
30	0.10%	0.50%	1.90%	7.50%	13.20%	20.70%	28.80%	36.30%
50	0.00%	0.0%	0.2%	1.00%	2.20%	5.3%	9.2%	12.0%